Published in final edited form as:

Cell Rep. 2024 September 24; 43(9): 114665. doi:10.1016/j.celrep.2024.114665.

Trigeminal innervation and tactile responses in mouse tongue

Linghua Zhang[1], **Maximilian Nagel**[2], **William P. Olson**[1], **Alexander T. Chesler**[2], **Daniel H. O'Connor**[1,3,*]

[1]Solomon H. Snyder Department of Neuroscience, Krieger Mind/Brain Institute, Kavli Neuroscience Discovery Institute, The Johns Hopkins University School of Medicine, Baltimore, MD 21218, USA

[2]Sensory Cells and Circuits Section, National Center for Complementary and Integrative Health, Bethesda, MD 20892, USA

[3]Lead contact

SUMMARY

The neural basis of tongue mechanosensation remains largely mysterious despite the tongue's high tactile acuity, sensitivity, and relevance to ethologically important functions. We studied terminal morphologies and tactile responses of lingual afferents from the trigeminal ganglion. Fungiform papillae, the taste-bud-holding structures in the tongue, were convergently innervated by multiple Piezo2$^+$ trigeminal afferents, whereas single trigeminal afferents branched into multiple adjacent filiform papillae. *In vivo* single-unit recordings from the trigeminal ganglion revealed lingual low-threshold mechanoreceptors (LTMRs) with distinct tactile properties ranging from intermediately adapting (IA) to rapidly adapting (RA). The receptive fields of these LTMRs were mostly less than 0.1 mm^2 and concentrated at the tip of the tongue, resembling the distribution of fungiform papillae. Our results indicate that fungiform papillae are mechanosensory structures and suggest a simple model that links functional and anatomical properties of tactile sensory neurons in the tongue.

Graphical Abstract

*Correspondence: dan.oconnor@jhmi.edu.

AUTHOR CONTRIBUTIONS

Conceptualization, L.Z., W.P.O., and D.H.O. Methodology, L.Z., W.P.O., and D.H.O. Investigation, L.Z. and M.N. Formal analysis, L.Z. Writing – original draft, L.Z. Writing – review & editing, L.Z., M.N., W.P.O., A.T.C., and D.H.O. Funding acquisition, A.T.C. and D.H.O. Supervision, A.T.C. and D.H.O.

DECLARATION OF INTERESTS

The authors declare no competing interests.

SUPPLEMENTAL INFORMATION

Supplemental information can be found online at https://doi.org/10.1016/j.celrep.2024.114665.

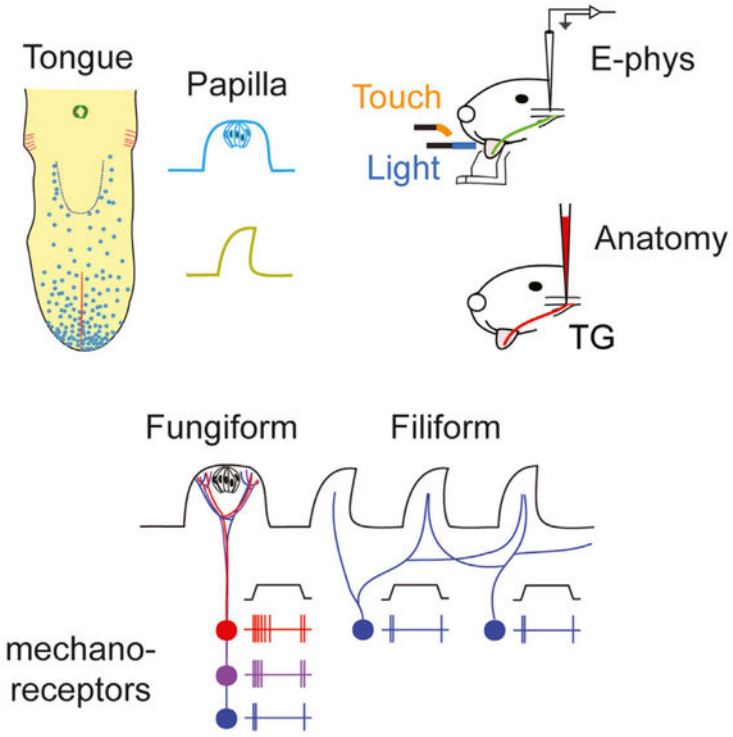

In brief

The tip of the tongue, one of the most tactile-sensitive areas in the body, is enriched with taste-bud-containing fungiform papillae. Zhang et al. reveal that fungiform papillae are touch sensors and suggest a model linking functional and anatomical properties of tactile sensory neurons in the tongue.

INTRODUCTION

The sense of touch is crucial for the function of the mammalian tongue in numerous behaviors, including chewing,[1] swallowing,[2,3] social grooming,[4] and vocalizing.[5,6] Tactile information from the tongue is often closely associated with chemo- and thermosensory inputs from food and drink. The tactile acuity and sensitivity of the human tongue outperforms that of the fingertips, with lower two-point discrimination thresholds and lower mechanical thresholds.[7–10] However, compared to touch-sensitive organs like the hands/paws and whiskers,[11] the neuronal subtypes and local terminal architectures underlying tactile sensitivity in the tongue are less well characterized.

The dorsal surface of the tongue, which contacts food and drink, is covered with stratified squamous epithelium and contains four types of protrusions called papillae: filiform, fungiform, circumvallate, and foliate, with filiform and fungiform the most abundant[12,13] (Figure S1). The mouse tongue has over 7,000 conical-shaped filiform papillae covering almost its entire dorsal surface.[14] Less abundant, mushroom-shaped fungiform papillae host

taste buds, and are concentrated at the tip and sides of the tongue. Based on their shape and abundance, filiform papillae have been hypothesized to be responsible for receiving tactile input[15–17] and to act either as strain sensors or strain amplifiers.[18] However, the observations that sensory afferents expressing the mechanotransduction channel Piezo2[19,20] can be found in both filiform and fungiform papillae,[21] and that the density of fungiform papillae is positively correlated with lingual tactile sensitivity in humans,[22–25] suggests that fungiform papillae may also be involved in touch sensation. Complicating the matter, a group of fibers in the chorda tympani, a branch of the facial nerve that carries taste information from the taste buds, can also respond to tongue stroking.[26,27] Questions about how the filiform and fungiform papillae are innervated by somatosensory neurons from the trigeminal ganglion (TG), how lingual low-threshold mechanoreceptors (LTMRs) respond to different tactile stimuli, and whether tactile nerve terminals form sensory end organs in the tongue remain to be answered.

We approached these questions using single-unit recordings from TG lingual LTMRs in anesthetized mice together with genetic labeling and tracing experiments. Our results uncover two groups of lingual LTMRs that differ in their tactile response properties, and suggest a model of how these two groups of LTMRs innervate different types of papillae and convey different information about touch on the tongue.

RESULTS

Trigeminal innervation of the tongue

To investigate how papillae are innervated by trigeminal neurons, we did DiI (1,1′-dioctadecyl-3,3,3′,3′-tetramethylindocarbocyanine perchlorate) anterograde tracing from the TG and examined the entire dorsal surface of the tongue in mice from postnatal day (P)0 to P21 (n = 10). We found that both fungiform papillae (Figures 1A and 1B, triangles, and 1C) and filiform papillae (Figures 1A and 1B, arrows, 1D) were innervated by trigeminal afferents, and that the tongue tip had the highest innervation density (Figure 1E). The efficiency of DiI tracing decreased at P21, as indicated by the lower signal-to-noise ratio in P21 in Figure 1E, with peaks of fluorescence representing the locations of fungiform papillae much higher in P21 compared to P10 and P12. Surprisingly, fungiform papillae, the taste-bud-holding structures concentrated at the anterior region of the tongue, were significantly more heavily innervated by trigeminal afferents than the uniformly distributed filiform papillae (Figure 1B). In comparison, previous studies suggest that the chorda tympani afferents from the geniculate ganglion (GG), which consist of gustatory fibers primarily and a subset of thermo- or mechanosensory fibers,[27,28] only innervate fungiform papillae.[29] Together, these findings suggest that the innervation pattern of TG afferents differs from that of GG afferents, and that both types of lingual papillae may be involved in somatosensation (Figure 1F).

Trigeminal and Piezo2^{+} innervation of the fungiform papillae

The longitudinal view of a fungiform papilla in Figure 1C shows that trigeminal afferents in a fungiform papilla penetrated the apical epithelium surrounding the taste pore and terminated in the extragemmal (outside of taste buds) region. To further explore the terminal

organization of trigeminal afferents in fungiform papillae, we examined fungiform papillae in confocal z-stacks to better appreciate how the axons traveled through the papillae. We found that the trigeminal fibers exhibit a ring-like termination pattern in fungiform papillae (Figure 2A), with little DiI signal in the middle part of the papillae, where taste pores and taste buds were located. The trigeminal nerve fibers innervating a fungiform papilla met at the base of the connective tissue and entered the connective tissue core as a bundle (Figure 2B, sections 1–3; Video S1). The clusters of nerve fibers then bifurcated into multiple branches, traveled toward the sidewalls of the papilla, and avoided the taste bud (Figures 2B, sections 4–7), while still going upward beyond the level of the taste bud until reaching the apical epithelium surrounding the taste pore, forming a ring-shaped terminal organization (Figure 2B, section 8). This finding is consistent with the description of the trigeminal innervation pattern in fungiform papillae in a previous study,[30] and their termination at the superficial epithelium suggests that the fungiform papillae innervating trigeminal afferents are capable of detecting sensory stimuli, including mechanical stimuli, in an extremely sensitive manner. We also found that the distribution of trigeminal afferents was asymmetric along the fungiform circumference. In both left and right sides of the tongue, the innervation was more concentrated in the posterior region of the fungiform papillae than in the medial/lateral regions (Figure 2C).

To investigate the innervation pattern of mechanosensitive afferents expressing Piezo2, we examined the dorsal surface of the tongue in *Piezo2-EGFP-IRES-Cre/+;Snap25*$^{LSL\text{-}EGFP/+}$ mice aged P1–P2 ($n = 4$) and *Piezo2-EGFP-IRES-Cre*/+ mice injected with AAV9-pCAG-FLEX-tdTomato virus intraperitoneally at ages P1–P2 ($n = 4$) to avoid lineage problems caused by embryonic expression of Piezo2. As with DiI-labeled trigeminal afferents, fluorescently labeled Piezo2^{+} afferents were found in both fungiform and filiform papillae but not in *Piezo2-EGFP-IRES-Cre/+;Snap25*$^{+/+}$ littermates (Figure 2D), suggesting that both types of papillae are involved in mechanosensation. Afferents expressing Piezo2 in fungiform papillae also exhibited a ring-like termination pattern and innervated the extragemmal region rather than the intragemmal (inside taste buds) region (Figure 2E, arrows; see also Figure 3C, bottom row, arrowhead), similar to DiI-labeled trigeminal afferents (Figure 1C). Considering that GG afferents are not the major contributor to extragemmal afferents in fungiform papillae,[26,31] our results suggest that TG afferents are the main mechanosensory supply for fungiform papillae.

Terminal morphology of lingual afferents

Sensory end organs are specialized structures formed at the terminals of sensory afferents that can act as mechanical filters and thus affect the mechanosensory responses of the axons. We next sought to describe any sensory end organs in the mouse tongue, with a special focus on the filiform papillae, where sensory innervation is solely provided by trigeminal afferents.

We found that both filiform papillae and fungiform papillae in the mouse tongue are innervated by neurofilament heavy chain (NFH)-positive myelinated afferents, consistent with prior work[17,21] (Figures 3A and S2). To visualize the shape of terminal Schwann cells, which are often involved in the structure of sensory end organs, we used immunostaining (S100β) and genetic labeling (*Plp1-EGFP*) methods targeting terminal Schwann cells. In

contrast to the glabrous skin, where we easily identified corpuscular end organs such as Meissner corpuscles (Figure 3A, bottom), we could not find corpuscular end organs (e.g., structures resembling the end bulbs of Krause or Meissner corpuscles in shape) in the filiform papillae of the mouse tongue (Figure 3A, top). The lack of Merkel cells at the apical epithelium of the tongue reported by other research groups[21,26] also suggests that the nerve terminals ascending the connective tissue cores of papillae were not likely to be associated with Merkel cells.

By conducting a small-scale screen of Cre mouse lines (Table S1), we identified several Cre lines that can label neuronal afferents on the surface of the tongue, including *Pirt*^{Cre}, *Vglut2*^{Cre}, and *Split*^{Cre}, which allowed us to better visualize the afferent terminals with genetic labeling strategies. In both *Pirt*^{Cre}*;Plp1-EGFP;R26*$^{LSL\text{-}tdTomato}$ and *Vglut2Cre;Plp1-EGFP;R26*$^{LSL\text{-}tdTomato}$ mice, tdTomato-labeled, myelinated, as well as unmyelinated primary afferents can be found in both fungiform papillae and filiform papillae. The terminal Schwann cells in mouse filiform papillae did not arrange in a compact stack and form either oval or cylindrical structures overall as in sensory corpuscles; rather, they merely formed a myelin sheath, which went missing before reaching the terminations of lingual afferents, leaving the nerve endings free (Figures 3B and 3C, triangles). In fungiform papillae, Vglut2^{Cre} labeled at least two different groups of afferents defined by their terminal locations: the intragemmal afferents innervating the taste bud (Figure 3C, arrowhead) and the extragemmal afferents that penetrated the apical epithelium surrounding the taste pore (Figure 3C, thick arrows). The terminals of both fungiform groups also did not associate with any PLP1-EGFP^{+} corpuscular structures. In *Split*^{Cre}*;Plp1-EGFP; R26*$^{LSL\text{-}tdTomato}$ mice, tdTomato-labeled unmyelinated primary afferents with free nerve endings were found in both fungiform papillae and filiform papillae (Figure 3D, arrows), which may represent nociceptors with lower conduction velocities.

The average size and the shape of tongue filiform papillae vary across mammalian species, as do their degrees of keratinization and structural complexity. Previous studies identified the existence of a type of simple corpuscle through immunohistochemistry and electron microscopy in the more developed filiform papillae of cats and cattle,[17,32] but not in the smaller and simpler filiform papillae of rats.[17] Contrary to previous findings suggesting the existence of a type of simple corpuscle called Krause end bulbs in the mouse tongue,[21] we could only find unencapsulated nerve endings in both types of papillae in mice.
To provide comparative context and test our ability to identify lingual end organs, we examined nervous elements in the ferret. Ferrets, similar to cats, are carnivorans, and their filiform papillae exhibit a more intricate structure, with secondary processes projecting from the main papilla.[33] We found that the majority of nerve afferents in the ferret tongue were not associated with corpuscles. However, unlike in the mouse tongue, ferret filiform papillae contained end organ structures with varied shapes, including cylindrical or globular structures that resembled the Krause end bulbs in cats (Figure S3, top and center). Individual filiform papillae could contain more than one end organ (Figure S3, bottom). Moreover, the lingual afferents encapsulated in a corpuscle usually had enlarged, blunt nerve endings (Figure S3, all three panels), and could branch at the terminal (Figure S3, bottom). Collectively, these results demonstrate that our methods allow us to identify sensory end

organs, highlight structural differences among filiform papillae of different animal species, and show that those of the mouse lack obvious sensory end organs.

Response properties of lingual LTMRs

We first determined the location of tongue-innervating neurons in the TG by retrograde DiI tracing from the tip of the tongue. We found that TG neurons innervating the tip of the tongue were mostly located near or at the ventral side of the TG mandibular branch rather than the dorsal side (Figure S4A), as significantly fewer tongue neurons (soma size of ≥20 μm) could be visualized at the dorsal TG by fluorescence microscopy (Figure S4B, dorsal: 14.9 ± 14.2, ventral: 71.3 ± 40.4; $p = 0.0011$, paired t test; $n = 9$ TG from 5 mice). The ventral location of the tongue neurons within the TG makes them amenable to single-unit recordings but possibly challenging targets for optical monitoring. In contrast, whisker pad-innervating TG neurons could be found in abundant numbers at both the dorsal and ventral sides of the TG (Figure S4A).

To make single-unit recordings, the tongue of an anesthetized mouse was carefully pulled out of the mouth using blunt forceps and placed on a stable slope, against which the lower teeth were braced to keep the mouth open during recordings (Figure 4A). The surface of the tongue was gently stimulated using a fine-tip brush until the activity of a unit that was responsive to brush strokes was captured by the electrode in the TG. The stable platform setup prevented tongue stimulation from causing unintended, correlated movements of the jaw and the lower chin as well as any potential mechanical stimulation of facial hairs on the lower face, which could lead to spurious inclusion of non-tongue units.

Using von Frey filaments to apply a constant force on their receptive fields (RFs), we found lingual LTMRs with different adaptation properties, ranging from the rapidly adapting (RA) to intermediately adapting (IA). Except for a few units that exhibited low spontaneous activity, none of the tongue units behaved like classic slowly adapting (SA) units that could fire continuously from touch onset to offset, such as those in the whisker system (Figure 4B). As all tongue units showed a certain amount of adaptation to touch stimuli, here, we define RA-LTMRs in the tongue as those that stopped firing roughly within 0.5 s in response to all tested von Frey stimuli (see STAR Methods), and IA-LTMRs otherwise. We found that the majority of lingual LTMRs had small RFs (less than 0.1 mm^2). Most LTMRs recorded had their RFs located either within 0.5 mm of the tip of the tongue (53.8%; Figure 4C) or along the midline or edge of the tongue, resembling the distribution of taste buds.

We examined the adaptation properties of the tongue LTMR population by comparing their average firing duration and adaptation index (AI) under a static force of 3.9 mN. Here, the AI was defined as the cumulative firing rate within an initial time period from touch onset divided by the total cumulative firing rate. The closer the AI is to 1, the faster the unit adapts, indicating a more rapid decrease in the firing rate over time. We observed that the level of adaptation across the neuronal population could be seen as a continuum (Figures 4D–4F and S5), and that the IA and RA units had similar firing rates at the stimulus onset but different speeds of adaptation in later phases (Figure 4G).

Apart from adaptation speed, lingual LTMRs also differed in their tactile sensitivity. Although lingual LTMRs in general had very low thresholds for static indentation, often less than 1.6 mN, RA-LTMRs usually had higher thresholds than IA-LTMRs. The thresholds for IA-LTMRs were consistently below 0.4 mN (Figure 4H), with some units registering as low as 0.2 mN (5 units) or 0.08 mN (1 unit, data not shown). Lingual LTMRs generally exhibited an elevated initial firing rate, with increasing static force application. However, the IA-LTMRs, which were more sensitive, tended to reach saturation in their firing rates at lower forces compared to the less sensitive RA-LTMRs (Figure 4I).

To measure the conduction velocity of lingual LTMRs, we first estimated the distance between the anterior part of the tongue to the TG through lingual nerve dissection and retrograde DiI tracing. By exposing the lingual nerve posterior to its exit from the tongue and cutting the nerve anterior to its entrance at the foramen ovale, we estimated an upper bound of the distance from the anterior part of the tongue to the TG in adult mice to be 1.8 cm. By injecting DiI at the tip of the tongue and using the known DiI traveling speed *in vivo* (6 mm/day),[34,35] we estimated a lower bound on the distance from tongue to TG to be 1.1 cm. These distances are short enough to limit proper measurement of fast axonal conduction velocity due to potential masking by electrical artifacts of the first induced neuronal spike during stimulation. Hence, we could only estimate the conduction velocity of lingual LTMRs as falling into the range of Aδ fibers (lower bound: 6.1 ± 2.7 m/s, higher bound: 9.9 ± 4.5 m/s; $n = 4$. Figure 4J) or above.

Lingual LTMRs were generally highly responsive to brush stroking, although their sensitivity to vertical force changes varied across the population. IA-LTMRs were highly sensitive to vertical forces as indicated by their extremely low thresholds. They were also sensitive to subtle force variations in the vertical direction. When indented by a handheld brush, where the applied force was not constant, unlike with von Frey filaments, they could maintain firing throughout the entire stimulation period, resembling SA-LTMRs. In contrast, RA-LTMRs fired only at the onset and offset of the indentation when stimulated with a handheld brush (Figure 4K). RA-LTMRs were also sensitive to rapid changes in the buckling direction of von Frey filaments during indentation, even when the filaments used were below their thresholds for static indentation (Figure 4K). These observations suggest that RA-LTMRs were more sensitive to shear/tangential forces than to vertical forces.

As Pirt and Vglut2 were reported markers for GG neurons and primary sensory neurons, including non-LTMR cell types in both trigeminal and dorsal root ganglia,[36–43] we tested whether the neuronal afferents labeled by $Pirt^{Cre}$ or $Vglut2^{Cre}$ on the surface of the tongue partly originated from the TG and included LTMR afferents. We performed single-unit recordings in the TG of $Pirt^{Cre};R26^{LSL\text{-}ChR2}$ mice and $Vglut2^{Cre};R26^{LSL\text{-}ChR2}$ mice and recorded the responses of lingual LTMRs when their RFs were stimulated by 473-nm blue light (Figure 4L). A total of 87.5% of lingual LTMRs in $Pirt^{Cre};R26^{LSL\text{-}ChR2}$ mice (Figure 4M) and 100% of lingual LTMRs in $Vglut2^{Cre};R26^{LSL\text{-}ChR2}$ mice (Figure 4N) could be activated by blue light, suggesting that in addition to labeling GG neurons, $Pirt^{Cre}$ and $Vglut2^{Cre}$ can label lingual LTMRs in the TG. Together, our results indicate that $Pirt^{Cre}$ and $Vglut2^{Cre}$ can label myelinated lingual afferents whose cell bodies are located in the TG, and that $Vglut2^{Cre}$ can label for both lingual IA- and RA-LTMRs.

Branching patterns of lingual afferents

To investigate the terminal field patterns of lingual neurons in the TG, we injected either AAVPHP.S-CAG-FLEX-tdTom or rAAV1-CAG-FLEX-tdTom virus into the TG in *Vglut2*^{Cre} mice (n = 18), which allowed us to label a subset of mandibular branch neurons, including lingual LTMRs, in a series of labeling densities from sparse to dense (Figure 5A). In densely labeled samples, we found that fungiform papillae from the anterior to posterior parts of the tongue were more heavily labeled by tdTomato compared to filiform papillae, and that the tip of the tongue, where fungiform papillae had the highest density, was thus equipped with the most TG afferents (Figure 5B). By sparsely labeling only a few lingual neurons, we identified at least three types of terminals with various shapes that innervated different parts of the tongue. At the dorsal side of the tongue, TG afferents innervating filiform papillae showed distinct branching patterns compared to those innervating fungiform papillae. Specifically, a single TG afferent projected to a single fungiform papilla and branched inside the papilla, whereas those innervating filiform papillae branched into multiple filiform papillae located nearby. At the junction of dorsal and ventral epithelium where no papilla structures were present, we observed small circular endings with no branches (Figure 5C). We did not attempt to trace the terminals of small-diameter afferents that might represent unmyelinated nociceptors.

We further looked at the relationship of TG afferents innervating the same or nearby papillae structures in samples where more than a few afferents were labeled. We observed that multiple afferents innervating the same fungiform papillae could converge along their path toward the papillae, and that separate afferents within the same nerve bundle could diverge to innervate different fungiform papillae (Figure 5D, top and center). Notably, we did not find individual afferents that branched to project to multiple fungiform papillae. In comparison, afferents innervating filiform papillae could travel in the same nerve bundle and exhibit overlap in their projected targets, while having different branching patterns (Figure 5D, bottom). The filiform papillae co-innervated by one or a few afferents formed distinct clusters (Figure 5E). The sizes of such filiform clusters were significantly larger than the terminal fields of fungiform-innervating afferents (Figure 5F), suggesting a more restricted RF for the latter.

Lingual LTMRs are unimodal touch sensors

The mammalian tongue is a sensory surface where mechanosensation, thermosensation, and chemosensation closely interact. There are special forms of tactile perception that can be induced by certain chemicals in food, such as astringency caused by chemicals containing the galloyl groups, including tannic acid in green tea, red wine, and unripe fruits,[44] and numbing induced by hydroxy-α-sanshool in green Sichuan peppercorns from the *Zanthoxylum* species.[45] We tested whether lingual LTMRs can be directly activated by temperature changes and certain chemicals applied over their RFs (Figure 6A). We did not observe responses to rapid cooling in lingual LTMRs (Figure 6B), nor did we detect responses to tannic acid or (−)-epigallocatechin gallate (EGCG), which contain galloyl groups, applied at concentrations ranging from 100 to 1,000 μM on the surface of the tongue (Figure 6C). Although hydroxy-α-sanshool was shown to be able to interfere with the vibration detection ability of RA channels on the fingertip,[46] we did not find obvious

differences in the mean firing rates of lingual RA-LTMRs measured before and after the application of 1,300 μM hydroxy-α-sanshool (Figure 6D). RA-LTMRs also did not respond to the application of a commercial Kava drink on their RFs (Figure 6E), which contains extracts from the roots of *Piper methysticum* and induces numbing sensations on the human tongue within tens of seconds. Collectively, these results suggest that mouse lingual LTMRs cannot be directly stimulated at the nerve terminals by rapid cooling or certain chemicals that produce astringent or numbing sensations in humans, and are therefore likely unimodal touch sensors.

DISCUSSION

We combined neuronal tracing, genetic labeling, and single-unit recording methods to investigate the innervation of the tongue by trigeminal afferents and the response properties of different types of LTMRs in the tongue. We discovered broad innervation of both filiform and fungiform papillae by TG afferents, and found no evidence for sensory corpuscles at the lingual afferent terminals in mice. Adaptation properties of lingual LTMRs fell on a spectrum from classic RA types to IA types, with sensitivities and preferences differing across the population. Sparse labeling of lingual neurons revealed distinct terminal shapes and branching patterns based on the type of papillae innervated. Our results suggest a simple model that relates the physiological properties of lingual LTMRs to anatomically defined patterns of innervation in the dorsal tongue (Figure 7).

Fungiform papillae as end organs for touch

The fungiform papillae were traditionally considered to be solely gustation related until recently, when mechanosensory afferents in the chorda tympani that respond to stroking and Meissner corpuscle-resembling structures in human tongue were identified.[27,47] In mice, it has been known that fungiform papillae are innervated by NFH^+ myelinated afferents and TG afferents.[21,30] However, the relative abundance of TG innervation in fungiform vs. filiform papillae remained largely unexplored, as well as the physiological properties of fungiform papillae innervating TG afferents. Consequently, it has been assumed for a long time that filiform papillae are the primary mechanosensory organs of the tongue.[18]

Our study reveals that compared to filiform papillae, fungiform papillae are more heavily innervated by TG afferents. As TG afferents projecting to fungiform papillae follow a one-to-one projection mode, rather than the one-to-many projection mode for filiform papillae, more neurons are assigned to the innervation of individual fungiform papillae. The innervation scheme may be roughly ($N > 10^1$ or 10^2) TG neurons: 1 fungiform papilla, and ($N > 10^0$ or 10^1) TG neurons: ($N = 10–20$) adjacent filiform papillae. The focalized innervation in fungiform papillae also suggests an emphasis on touch inputs from them in the TG. Indeed, most lingual LTMRs we recorded from received touch information at the tip of the tongue, where fungiform papillae are most abundant. The locations of most lingual LTMRs' RFs also resembled those of fungiform papillae, especially those along the midline of the tongue. The small RFs of most lingual LTMRs and the high trigeminal innervation density of fungiform papillae may explain why the tip of the tongue has high tactile sensitivity. We speculate that fungiform papillae could serve as end organs for touch.

Comparison between lingual and hairy skin LTMRs

The organization of trigeminal nerve endings around two distinct types of papillae on the tongue resembles the way nerves are distributed around hair follicles in skin. In mice, there are different types of hairs on the skin. Guard hairs, making up ~1% of hair follicles, are individually innervated by Aβ SA-LTMRs, with each nerve ending terminating into a single guard hair. The more common zigzag and awl/auchene hairs, accounting for ~74% and ~25% of follicles, respectively, are innervated by LTMRs whose terminals cover a large area encompassing multiple hairs, including Aβ RA-LTMRs (innervate awl/auchene and guard hairs), Aδ-LTMRs, and C-LTMRs.[48,49] Similarly, our study revealed that the fungiform papillae, making up ~2% of lingual papillae, are innervated by potential lingual LTMRs with restricted terminal fields, each of which terminates exclusively at a single fungiform papilla. In contrast, the potential lingual LTMRs innervating the much more abundant filiform papillae (~98% of papillae) display a more diffused termination pattern, mimicking those of Aβ RA-, Aδ-, and C-LTMRs.

Our electrophysiological data suggest that lingual LTMRs have varied adaptation properties, sensitivities, and tactile preferences, which might result from the organization of their terminals and the mechanical characteristics of the tissues they innervate. Compared to the IA types, some of the RA types were less sensitive to indentation but equally responsive to brush stroking, resembling RA-LTMRs found in the hairy skin with lanceolate endings. Filiform papillae, being more keratinized than fungiform papillae, likely harbor the least indentation-sensitive lingual LTMRs, which predominantly consist of RA types. Conversely, LTMRs innervating fungiform papillae are expected to have lower thresholds (0.08–0.4 mN), including both IA- and RA-LTMRs (Figure 7).

In hairy skin, Aβ SA-LTMRs innervating the guard hairs are associated with Merkel cells.[50] In the mouse tongue, however, we did not find any SA-LTMR that could fire throughout the indentation period, except for only a few units with low spontaneous activities. Previous studies have shown that Merkel-neurite complexes may not be a major end organ in the mouse tongue,[21,26] although some keratin 20^+ cells (potential Merkel cells) associated with NFH^+ fibers were seen in the base of the ridges between filiform papillae.[26] It has also been shown that ablating or dysfunctioning Merkel cells in Merkel-neurite complexes can convert SA afferents into IA.[51,52] Therefore, it may not be surprising to see that lingual LTMRs without Merkel cell associations exhibit a spectrum of adaptation properties from RA to IA, but not SA.

TG and GG touch receptors

Previous studies show that GG neurons that can be labeled by the transcription factor Phox2b mainly terminate at the taste bud itself and make contact with taste bud cells, forming intragemmal projections.[31,53] A few $Phox2b^+$ afferents were also seen to innervate the extragemmal region of fungiform papillae. Those were hypothesized to be mechanosensitive chorda tympani fibers as they were preserved together with the mechanosensitivity of chorda tympani fibers after taste bud elimination.[26] However, most of the extragemmal afferents in fungiform papillae were not $Phox2b^+$, and $Phox2b^+$ extragemmal afferents were only seen in 43% of the fungiform papillae,[31] suggesting that

the extragemmal afferents in fungiform papillae may have a main source other than the GG. We observed that unlike the termination pattern of the GG, the TG afferents terminate at the Piezo2$^+$ afferents-enriched extragemmal region of fungiform papillae, suggesting that the majority of the extragemmal mechanosensory afferents have a trigeminal origin. This is consistent with previous findings showing that chorda tympani denervation had negligible effects on the extragemmal afferents.[54,55]

In summary, TG afferents have a largely different innervation pattern compared to GG afferents. First, TG afferents provide somatosensory innervation to filiform papillae, which are not supplied by GG afferents. Second, the termination patterns of TG and GG afferents in fungiform papillae are largely non-overlapping. The TG nerve terminals occupy the Piezo2$^+$ afferents-enriched extragemmal space in the apical epithelium, while the majority of GG nerve terminals reside in the intragemmal space, with a few putatively mechanosensitive exceptions. This suggests a functional specialization in the nerve fibers innervating different regions of the fungiform papillae.

Modality specificity of lingual LTMRs

Previous work has shown that cutaneous C- and Aδ-LTMRs can be stimulated by rapid cooling of the skin.[50] A recent study using *in vivo* calcium imaging of mouse trigeminal neurons also identified lingual mechanosensory neurons that were responsive to cooling.[56] Here, our experimental setup and the range of force stimuli were chosen to ensure that only lingual LTMRs were recorded, excluding potential multimodal nociceptors and neurons innervating deeper tissues. In particular, our sample of lingual LTMRs was insensitive to cooling on the tongue surface, consistent with previous findings showing that both Aδ and Aβ lingual mechanoreceptors in rats are specialized touch sensors with no response to either cold or warm stimuli (8°C–51°C) or menthol.[57] This can be explained by the lack of Trpm8 (involved in cooling sensation[58]) expression in the vast majority of Piezo2$^+$ trigeminal neurons revealed by single-cell RNA sequencing and *in situ* hybridization[59,60] and lack of mechanical response in Trpm8-expressing trigeminal neurons.[59]

Our sample of tongue LTMRs was not directly stimulated by chemicals that induce astringent or numbing sensations. However, previous work found that some TG neurons can be activated by astringent compounds, including tannic acid or EGCG *in vitro*.[44] We think that these neurons might be chemosensory or polymodal neurons and that it is worthwhile to perform *in vitro* chemical tests on Piezo2-expressing TG neurons.

Limitations of the study

Although we did not find sensory end organs resembling any known type at the dorsal surface of the mouse tongue, lingual LTMRs may be associated with terminal structures that we did not examine, such as collagen fiber structures. The potential association of lingual nerve terminals with collagen fibers may also affect their tactile response properties, and could be studied using electron microscopy.

Our model of tongue mechanosensation proposes that LTMRs with lower thresholds (below 0.4 mN) innervate the fungiform papillae. This can be directly tested by stimulating a single fungiform papilla during TG recordings. In rat tongue, the fungiform papillae are big enough

to enable precise stimulation of a single papilla.[28] In mice, the tiny fungiform papillae can be visualized with food dyes but will require a precise apparatus to allow stimulation while avoiding nearby filiform papillae (Figure S6).

We found one IA-type unit with a significantly larger RF. This outlier raises the possibility that there are novel terminal types that we have not described, perhaps occupying a large area in the manner of field LTMRs in hairy skin,[61] but with indentation responses different from those of skin field LTMRs.

Finally, our study did not explore the behavioral importance of lingual IA- and RA-LTMRs, and we did not compare the functional importance of TG and GG mechanoreceptors innervating the tongue. It will be important to modulate the activity of LTMRs by optogenetic activation or inhibition acutely, or to ablate LTMR populations using genetic strategies to see whether the orofacial behaviors of the animals are affected. It would also be interesting to study whether a change in the filiform papillae patterning will affect animals' touch senses on the tongue by using transgenic mouse lines with altered filiform papillae patterns.[14]

RESOURCE AVAILABILITY

Lead contact

Further information and requests for resources and reagents should be directed to and will be fulfilled by the Lead Contact, Daniel H. O'Connor (dan.oconnor@jhmi.edu).

Materials availability

This study did not generate new unique reagents.

Data and code availability

- Data in MATLAB (.mat) and.csv formats have been deposited at Zenodo and are publicly available as of the date of publication. DOIs are listed in the key resources table.
- All original code has been deposited at Zenodo and is publicly available as of the date of publication. DOIs are listed in the key resources table.
- Any additional information required to reanalyze the data reported in this paper is available from the lead contact upon request.

STAR★METHODS

Detailed methods are provided in the online version of this paper and include the following:

EXPERIMENTAL MODEL AND STUDY PARTICIPANT DETAILS

Mice—All procedures were in accordance with protocols approved by the Johns Hopkins University Animal Care and Use Committee (protocols: MO18M187 and MO21M195). Mice of both sexes were used for experiments. For DiI tracing experiments, mice aged from P0 to P21 from both C57BL/6 and CD1 backgrounds were used. For the other experiments,

adult mice aged from 6 weeks to 12 months from C57BL/6 background were used, and the mouse lines used in this study included: *Plp1-EGFP* (B6; CBA-*Tg(Plp1-EGFP) 10Wmac/J*), *Piezo2-EGFP-IRES-Cre* (B6(SJL)-*Piezo2*$^{tm1.1(cre)Apat}$/J), *Snap25-LSL-2A-EGFP-D* (B6.Cg-*Snap25*$^{tm1.1Hze}$/J), *Vglut2*^{Cre} (B6J.129S6(FVB)-*Slc17a6*$^{tm2(cre)Lowl}$/MwarJ), *Rosa26*^{Ai9} (B6.Cg-*Gt(ROSA)26Sor*$^{tm9(CAG-tdTomato)Hze}$/J), *Rosa26*^{Ai14} (B6.Cg-*Gt(ROSA)26Sor*$^{tm14(CAG-tdTomato)Hze}$/J), *Rosa26*^{Ai32} (B6; 129S-*Gt(ROSA)26Sor*$^{tm32(CAG-COP4*H134R/EYFP)Hze}$/J), *TrkB*^{CreERT2} (B6.129S6(Cg)-*Ntrk2*$^{tm3.1(cre/ERT2)Ddg}$/J), *TrkC*^{CreERT2} (*Ntrk3*$^{tm3.1(cre/ERT2)Ddg}$/J), *Etv1*^{CreERT2} (B6(Cg)-*Etv1*$^{tm1.1(cre/ERT2)Zjh}$/J), *Vglut1*$^{IRES-Cre}$ (B6; 129S-*Slc17a7*$^{tm1.1(cre)Hze}$/J), *Advillin*^{Cre} (B6.129P2-*Avil*$^{tm2(cre)Fawa}$/J), *PV*^{Cre} (B6; 129P2-*Pvalb*$^{tm1(cre)Arbr}$/J), *TH*^{Cre} (B6.Cg-*7630403 G23Rik*$^{Tg(Th–cre)1Tmd}$/J), *MafA*^{Cre},[62] P*irt*^{Cre},[40] and *Split*^{Cre}.[63]

To induce CreER-based recombination, tamoxifen was given either in the embryonic stage or to newborn pups. For embryonic stage, a mixture of tamoxifen (3 mg, Toronto Research Chemicals, T006000), progesterone (MilliporeSigma, P0130) and β-estradiol (MilliporeSigma, E8875) in 1:0.5:0.001 ratio prepared in sunflower seed oil (MilliporeSigma, S5007) was administered by oral gavage to pregnant dams. Pups were delivered by Caesarian section at E19-E19.5 and reared by a CD1 foster mother. For newborn pups, 0.1 mg tamoxifen in sunflower seed oil was injected intraperitoneally. The ages of mice when the drug was administered are summarized in Table S1.

Ferret—The tongue tissue of an 8-month-old ferret was used for histological analysis.

METHOD DETAILS

Histology—Mice were perfused with PBS transcardially followed by 4% PFA. The tissue was further fixed in 4% PFA at 4°C overnight, and washed in PBS 3 times afterward.

H&E staining: The tissue was dehydrated in 30% sucrose in PBS at 4°C overnight, and protected by OCT embedding compound (4583, Sakura) before being frozen. The tissue was then cryo-sectioned into 8–10 μm sections on a Leica cryostat. Sections were hydrated in deionized water, stained in Mayer's Hematoxylin Solution (MHS1, Sigma-Aldrich) for 15 min, rinsed in warm running tap water for 15 min, then placed in distilled water for 30 s followed by 95% Reagent Alcohol for 30 s. The sections were then placed in Eosin Y Solution (HT110216, Sigma-Aldrich) for 30–60 s. Afterward, they were dehydrated and cleared through 2 changes of 95% Reagent Alcohol, Reagent Alcohol and xylene for 2 min each. The sections were mounted with Balsam Canada Neutral in xylene (846578, Carolina Biological Supply Company), and imaged with a Keyence microscope using brightfield illumination.

Masson-Goldner trichrome staining: The tissue was dehydrated in 30% sucrose in PBS at 4°C overnight, and protected by OCT embedding compound before being frozen. The tissue was then cryosectioned into 8–10 μm sections on a Leica cryostat. Sections were hydrated in deionized water, stained with a Masson-Goldner staining kit (1.00485, Sigma-Aldrich). The sections were mounted with Balsam Canada Neutral in Xylene (846578, Carolina Biological Supply Company), and imaged with a Keyence microscope using brightfield illumination.

Immunostaining: The tissue was dehydrated in 30% sucrose in PBS at 4°C overnight, and protected by OCT embedding compound before frozen. The tissue was then cryo-sectioned into 9–40 μm sections on a Leica cryostat. Sections were rehydrated in PBS, permeabilized and blocked by 10% goat serum in 0.3% PBST solution (0.3% Triton X-100 (MilliporeSigma, T9284) in PBS) for 1 h at room temperature, then incubated with primary antibodies diluted in blocking solution (5% goat serum in 0.3% PBST) at 4°C overnight. The sections were washed by 0.3% PBST at least 3 times, 15 min each before incubation with secondary antibodies and DAPI diluted in blocking solution at 4°C overnight. The tissue was finally washed by 0.3% PBST at least 3 times and PBS 1 time, mounted with Poly Aqua-Mount (Polysciences, 18606), and imaged using a confocal microscope (Zeiss LSM 880 or Zeiss LSM 700).

Whole-mount imaging of DiI-labeled tongue tissue: In P1-P10 mice, after fixation, muscles at the ventral side of the tongue were carefully removed by hand with a surgical blade. The tissue was then mounted dorsal side down on a 30 mm × 10 mm tissue culture dish with 15 mm glass bottom (Celltreat, 229632) in Poly Aqua-Mount. A coverslip was placed on the tissue to gently flatten it. It was then imaged with a wide-field microscope (Zeiss Axio Zoom) or a confocal microscope (Zeiss LSM 880). After whole-mount imaging of the dorsal surface, the tissue was cryo-sectioned. The sections were immediately washed with PBS, mounted with Poly Aqua-Mount and imaged using a confocal microscope (Zeiss LSM 880) after sectioning before DiI diffusion post-cut.

Whole-mount imaging of tdTom-expressing tongue tissue post-viral injection: After fixation, muscles at the ventral side of the tongue were carefully removed by hand with a surgical blade. The tissue was then cleared by CUBIC Protocol I as described, which can preserve endogenous fluorescent proteins during clearing.[65] Briefly, after fixation and washing of the tissue, the tissue was immersed in CUBIC L solution (10% w/v N-butyldiethanolamine (MilliporeSigma, 471240) and 10% w/v Triton X-100 in water) for 3 days at 37°C. It was then washed in PBS overnight at room temperature, followed by immersion in 50% water-diluted CUBIC R solution (45% w/v antipyrine (Tokyo Chemical Industry, D1876) and 30% w/v nicotinamide (Tokyo Chemical Industry, N0078) in water) at room temperature for 1 day. Finally, it was immersed in the CUBIC R solution at room temperature for 1–2 days. All steps were done with gentle shaking. The tissue was imaged with a wide-field microscope (Zeiss Axio Zoom or Olympus BX-41) or a confocal microscope (Zeiss LSM 700). For confocal imaging, the tissue was mounted dorsal side down on a 30 mm × 10 mm tissue culture dish with 15 mm glass bottom in CUBIC R solution. A coverslip was placed on the tissue to gently flatten it.

Whole-mount imaging of immunostained NFH: The dorsal surface of the tongue was flattened using a method modified from Wang et al. (2016).[14] Freshly dissected tongue was put dorsal side down into a 3-D printed reservoir and was gently pressed against the bottom of the reservoir by a cell strainer (Fisher Scientific, 22-363-549). 4% PFA was added into the reservoir to fix the tissue at 4°C overnight. The flattened tongue was then fixed for another 1 h at room temperature, washed in PBS 3 times, embedded in agarose, and its dorsal part was cut into 300 μm sections using a vibratome (HM 650V, Thermo Scientific).

The tissue was then stained and cleared using iDISCO method.[66] Briefly, the tissue was pretreated with a series of methanol/water (20%, 40%, 60%, 80%, 100%) for 1 h each, then washed further with 100% methanol (MilliporeSigma, 676780) for 1 h and chilled at 4°C. It was then incubated in 66% dichloromethane (MilliporeSigma, 270997)/33% methanol overnight at room temperature with shaking, washed twice in 100% methanol at room temperature on the next day, and chilled at 4°C. Then it was bleached in chilled fresh 5% (v/v) hydrogen peroxide (MilliporeSigma, HX0640) in methanol overnight at 4°C, rehydrated with methanol/water series on the next day, and washed in PTx.2 (0.2% Triton X-100 in PBS) for 1 h at room temperature 2 times. The tissue was then permeabilized by permeabilization solution (23 g/L glycine (MilliporeSigma, G7126) and 20% DMSO (MilliporeSigma, 472301) in PTx.2) at 37°C for 2 days, blocked by blocking solution (6% normal goat serum and 10% DMSO in PTx.2) at 37°C for 2 days, incubated with 1:1000 Chicken anti-NFH in PTwH (0.2% Tween 20, 10 mg/L heparin in PBS)/5%DMSO/3% normal goat serum at 37°C for 7 days, washed in PTwH at 37°C 4–5 times until the next day, followed by incubation with 1:500 Goat anti-Chicken IgG Alexa Fluor 647 in PTwH/5%DMSO/3% normal goat serum at 37°C for 7 days and washing in PTwH at 37°C 4–5 times until the next day. Finally, the tissue was dehydrated with methanol/water series for 1 h each at room temperature, incubated with 66% dichloromethane/33% methanol for 3 h with shaking at room temperature, and incubated in 100% dichloromethane for 15 min twice with shaking to wash away the methanol. The final dehydration steps and the washing steps were done in a Petri dish with the tissue sandwiched by two glass slides to preserve the flattened state of the tissue as much as possible. After that, the tissue was immersed in dibenzyl ether (MilliporeSigma, 108014) at room temperature for refraction index matching until it was cleared, and imaged with a confocal microscope (Zeiss LSM 880).

Primary antibodies used in this study and their dilution ratios or concentration were as follows: Chicken anti-NFH 1:1000 (MilliporeSigma AB5539), Rabbit anti-S100 1:50 (Abcam AB76729), Rabbit anti-S100 1:200 (ProteinTech, 15146-1-AP), Rabbit anti-PGP9.5 1:1000 (MilliporeSigma, AB1761-I).

Secondary antibodies used in this study and their dilution ratios were as follows unless otherwise stated: Goat anti-Rabbit IgG Alexa Fluor 488 1:1000 (ThermoFisher A-11008), Goat anti-Rabbit IgG Alexa Fluor 594 1:1000 (ThermoFisher A-11012), Goat anti-Rabbit IgG Alexa Fluor 647 1:1000 (ThermoFisher A-21244), Goat anti-Chicken IgG Alexa Fluor 488 1:1000 (ThermoFisher A-11309), Goat anti-Chicken IgG Alexa Fluor 647 1:1000 (ThermoFisher A-11039), Goat anti-Rat IgG Alexa Fluor 647 1:1000 (ThermoFisher A-21247).

DiI tracing

Anterograde tracing: For anterograde DiI tracing from TG to tongue, the DiI crystal labeling procedure was modified from Fei et al. (2014).[29] Briefly, after perfusing mice aged P0 - P21 with PBS and 4% PFA, the brain was removed to expose the TG. The dura covering the mandibular branch of TG was pierced through with #5 forceps. DiI (1,1′-dioctadecyl-3,3,3′,3′-tetramethylindocarbocyanine perchlorate ($DiIC_{18}(3)$), Invitrogen D282) crystals were implanted into the mandibular region on both left and right sides of the

TG, and a few drops of 100% ethanol were added onto the region to dissolve DiI. The head, with the tongue and the TG left *in situ*, were covered by a wet paper towel for half an hour, then placed in 4% PFA and incubated at 37°C for 6 months before the tongue tissue was harvested. In another set of experiments (Figure 1E), mice aged P10 - P21 were used and their tissue was incubated with DiI at 25°C–37°C for 18 months.

Retrograde tracing: For retrograde DiI tracing from the periphery to TG, $DiIC_{18}(3)$ crystals were dissolved in DMSO to create a 1 mg/mL solution. This solution was then diluted in PBS at a ratio of 1:5 to achieve a concentration of 0.2 mg/mL. 2.0 μL of the 0.2 mg/mL DiI solution was injected either into the tip of the tongue or the left whisker pad using a 1 μL micro-syringe (Hamilton) for somatotopic mapping. The animals were sacrificed 5–7 days after DiI injection to maximize neuronal labeling. To estimate the distance between the tip of the tongue and the TG, 2.0 μL of the 0.2 mg/mL DiI solution was injected into the tip of the tongue, and the animals were sacrificed at 1 day, 1.5 days, 42 h, 45 h, 2 days, or 5 days after the injection.

Surgery—Adult mice (older than 8 weeks) were implanted with titanium head caps ahead of electrophysiological recordings or viral injections in TG. The anesthesia was induced with 3% isoflurane in O_2 and then maintained with 1.5% isoflurane. Mice were kept on a heat blanket (Harvard apparatus), and ophthalmic ointment was applied on eyes to keep them moisturized. 0.5% bupivacaine was locally injected under the scalp, and dexamethasone (2 mg/kg) was intraperitoneally injected to prevent inflammation. The skin and the periosteum over the dorsal surface of the skull were removed. A headcap was glued by cyanoacrylic gels (Krazy glue) onto the skull and fixed in place by dental cement. Mice were injected with buprenorphine SR (1 mg/kg s.c.) for analgesia and allowed to recover for 7 days. Following headcap implantation, a 2.3 × 2.3 mm cranial window was made with the center located at 2 mm posterior to bregma, 2 mm lateral to bregma. The exposed brain region was covered with a biocompatible silicone elastomer (e.g., Kwik-Cast, World Precision Instruments) after craniotomy.

***In vivo* TG electrophysiology—**Mice with head caps were anesthetized by ketamine/xylazine (87.5 mg/kg and 12.5 mg/kg, respectively, i.p.), head-fixed, and kept on a heating blanket to maintain body temperature. The tongue was gently pulled out of the mouth with blunt forceps and put on a custom-made stable platform with an angle of 30° from the vertical, against which the lower teeth were braced to keep the mouth open during recordings. The accessible length of the tongue on the platform was 2.5–3 mm. The images of the tongue stained by food color dyes were captured with a circuit board USB digital microscope (Chipquick, SMDPMUSB413; Figure S6). To keep the surface of the tongue moisturized, artificial saliva (4 mM NaCl, 10 mM KCl, 6 mM $KHCO_3$, 6 mM $NaHCO_3$, 0.5 mM $CaCl_2$, 0.5 mM $MgCl_2$, 0.24 mM K_2HPO_4, 0.24 mM KH_2PO_4, pH 7.5)[67] at room temperature was applied on the tongue as needed. A 2 MΩ tungsten electrode (World Precision Instruments, TM33A20) driven by a Sutter manipulator was inserted into the depth of TG (around 5–6 mm below the brain surface). A ref. 2 MΩ electrode was placed outside the craniotomy covered in sterile saline. The differential signal between the recording and the reference electrodes was amplified 10,000x, band-pass filtered between

300 Hz and 3,000 Hz (DAM 80, World Precision Instruments), and acquired at 20 kHz using WaveSurfer (https://wavesurfer.janelia.org/). In order to find tongue units, multiple TG locations surrounding 2.3 mm posterior to bregma, 2 mm lateral to bregma were probed. While the electrode was moving down at the depth of TG, the orofacial regions of the mouse including whisker pad, cheek, lower jaw and tongue were touched by a hand-held fine-tip brush in a stroking manner to reveal the receptive fields of the units encountered. Once a unit that responded only to tactile stimuli on the tongue was discovered, it was further tested with von Frey filaments, chemicals, and ice-cold artificial saliva. Von Frey filaments were pointed perpendicular to the RF, and forces ranging from 0.08 mN to 9.8 mN were applied as follows. For units with RFs located away from the edge of the tongue, a range of von Frey stimuli ranging from 0.08 mN to 9.8 mN could be applied. For those with their RFs located at the edge of the tongue, where the local curvature of the tongue surface was significant, their responses to 9.8 mN (and sometimes 5.9 mN) were not tested due to a significant push of the tongue by the larger von Frey filaments. To test the conduction velocity of the unit, a 0.4 mA, 1 ms electric pulse generated by a stimulus isolator (World Precision Instruments, A365) was delivered onto the unit's receptive field by a concentric bipolar electrode (World Precision Instruments, TM33CCINS). For opto-tagging experiments, 10 ms light pulses were generated by a 473 nm DPSS laser (Laserglow Technologies, R471003GX) and delivered to the tongue via a 200 μm, 0.39 NA optical fiber manually positioned approximately 1 mm away from the unit's receptive field, with the actual power to be 15–18 mW. The TTL inputs sent to the stimulus isolator and the laser were generated from a National Instruments DAQ system and recorded by Wavesurfer together with electrophysiological data. When a unit was found with an RF located near the edge of the tongue, it was further probed with tactile and optical stimuli at both ventral and dorsal sides of the tongue to determine its exact RF location. The mice were re-dosed with 25–50% of the initial ketamine/xylazine dose once they started to wake up from anesthesia, as indicated by whisker twitching.

Chemicals applied on the tongue surface included: tannic acid (100, 200, 500, 1000 μM, diluted with artificial saliva, MilliporeSigma, 403040), (−)-epigallocatechin gallate (EGCG, 100, 200, 500, 1000 μM, diluted with artificial saliva, MilliporeSigma, E4143), Hydroxy-α-sanshool (1900 μM, freshly dissolved in DMSO and then diluted with artificial saliva by 1:20, Medchemexpress, HY-N6825), Kava concentrate (commercial drink, Kalm with Kava, iced tea flavor).

Viral injection in the TG—Glass pipettes (Wiretrol II, Drummond Scientific Company, 5–000-2010) with a long taper (more than 6 mm) were pulled using a pipette puller (Sutter Instruments, model P-97) for TG injection. The tips of the pipettes were then trimmed by forceps and beveled using a custom beveler. A custom microinjection system was used for injection. For sparse to dense labeling of mandibular branch neurons, the pipette containing AAVPHP.S-CAG-FLEX-tdTomato virus (Addgene 28306-PHP.S, 1.8×10^{13} vg/mL) was targeted to 1–4 injection sites spaced 150–200 μm apart in the mandibular branch (lateral 2.1–2.4 mm, posterior 2.2–2.5 mm relative to bregma). For each injection site, 0.2 μL virus was injected at a rate of 70 nL/min at a depth between 5.8 and 6 mm. The craniotomy was then covered and protected by silicon elastomer and the mice were sacrificed 3 weeks after

viral injection. In another set of experiments, rAAV1-CAG-FLEX-tdTomato virus (Addgene 45282, 1.2×10^{13} GC/mL) was injected into the TG mandibular branch. For dense labeling, a total of 1–1.2 μL of virus was injected at 4 locations spaced 150–200 μm apart. For sparse labeling, a total of 0.4–0.8 μL of virus was injected at 2 locations spaced 200 μm apart. The injection depths were 5.7–5.9 mm. The mice were sacrificed 4–4.5 weeks after viral injection.

Piezo2 expression of tongue-innervating neurons—Tongue tissue was collected from *Piezo2-EGFP-IRES-Cre/+;Snap25*$^{LSL\text{-}EGFP/+}$ mice at P1-P2 after decapitation and was freshly embedded in low-melt agarose (2% at 40°C) with the dorsal side facing up, followed by imaging with a confocal microscope. To avoid lineage problems caused by embryonic expression of Piezo2, other mice that were *Piezo2-EGFP-IRES-Cre/+;Snap25*$^{LSL\text{-}EGFP/+}$ or *Piezo2-EGFP-IRES-Cre/+;Snap25*$^{+/+}$ were injected with AAV9-pCAG-FLEX-tdTomato-WPRE interperitoneally (10 μL, 6.4×10^{12} GC/mL). The tissue was harvested 14 days after injections. The green autofluorescence and the tdTomato expression at the dorsal surface of the tongue were imaged with a confocal microscope. The autofluorescence signals from the filiform papillae were subtracted from the red channel with Fiji. AAV9-pCAG-FLEX-tdTomato-WPRE was a gift from Hongkui Zeng (Addgene plasmid # 51503) and was produced by Vigene Biosciences.

QUANTIFICATION AND STATISTICAL ANALYSIS

All analyses were performed using custom-written Python or MATLAB (MathWorks) scripts. The confocal and wide-field fluorescence images were processed using Fiji (ImageJ).

DiI intensity across the tongue—The fluorescence intensity of a 500 μm-wide square region of interest (ROI) with one edge located 150–200 μm away from the tip of the tongue to ensure that the ROI was entirely inside the tongue, and another edge aligned with the location of the farthest fungiform papilla at the posterior of the tongue, was analyzed using Fiji “Analyze - Plot Profile”. The averaged fluorescence intensity at each distance along the A-P axis was normalized according to the equation:

$$Normalized\ \ intensity = 100\ \frac{Intensity\ -\ min(Intensity)}{max(Intensity)\ -\ min(Intensity)}$$

The distance along the A-P axis was also normalized according to the equation:

$$Normalized\ \ distance = \frac{Distance\ -\ min(Distance)}{max(Distance)\ -\ min(Distance)}$$

Innervation intensity surrounding fungiform papillae—Confocal stacks of individual fungiform papillae innervated by DiI-labeled trigeminal afferents were analyzed using Fiji. Both sphere-shaped and ellipse-shaped fungiform papillae were included for the analysis. Image slices containing nerve fibers at the base of fungiform papillae were excluded for maximum intensity projection of the z-stacks. A circle or ellipse was drawn to fit the contour of the papillae, and the image was unwrapped and converted to polar

coordinates using the plugin “Polar Transformer” with 360° used for polar space and 1 line per angle. The fluorescence intensity of the outer ring region of fungiform papillae was selected as ROI and analyzed using “Plot Profile”. The fluorescence intensity at each angle for a specific fungiform papilla was normalized according to the equation:

$$Normalized\ \ intensity = 100\ \frac{Intensity\ -\ min(Intensity)}{max(Intensity)\ -\ min(Intensity)}$$

Spike sorting—Voltage recordings were high-pass filtered at 300 Hz using MATLAB R2023a (MathWorks), thresholded, and clustered using MClust 4.4 (A. D. Redish, https://github.com/adredish/MClust-Spike-Sorting-Toolbox) to extract single unit waveforms and spike times. Units whose RFs were located at the ventral side of the tongue were not analyzed.

Peristimulus time histogram (PSTH) and adaptation index—As the exact timing of von Frey hairs’ contact with the tongue could not be registered, the stimulus onset was determined by the timing of the first spike of a unit in response to von Frey stimulation. The 50 ms bin size was adopted after comparing the PSTH results using 10, 20, 30, 50 and 100 ms time bins. The adaptation index (AI_t) was first calculated using different criteria based on the estimated time taken for the 3.9 mN von Frey stimulus to reach a plateau (t = 150, 200, 250, and 300 ms), after which t = 250 and 300 were adopted. The AI_t was calculated by the equation:

$$AI_t = \frac{\sum_{i=1}^{t/50} Average\ \ firing\ \ rate\ \ in\ \ time\ \ bin\ \ (i)}{\sum_{i=1}^{T/50} Average\ \ firing\ \ rate\ \ in\ \ time\ \ bin\ \ (i)},$$

where T was the total duration of a spike train excluding the touch offset responses. Units with a low spontaneous activity ($n = 2$) were excluded for this analysis.

Neuroanatomical tracing and terminal field quantifications—Semi-automatic tracing of sparsely labeled trigeminal afferents was performed using the SNT toolbox (https://imagej.net/plugins/snt/). The terminal field sizes for afferents innervating fungiform papillae were determined by a convex hull enclosing all the endings and the afferent branching point near the fungiform papillae. For afferents innervating multiple filiform papillae, the terminal field included only a narrow area surrounding all the afferent branches near the terminal (not a convex hull).

Statistics—Unless otherwise noted we report data as mean ± SD; statistical tests were two-tailed; statistical hypothesis testing used $\alpha = 0.05$. No statistical methods were used to predetermine sample sizes.

Supplementary Material

Refer to Web version on PubMed Central for supplementary material.

ACKNOWLEDGMENTS

We thank Xinzhong Dong for $Pirt^{Cre}$ and $MafA^{Cre}$ mice, Wenqin Luo for $Split^{Cre}$ mice, Kristina Nielsen and Jennifer Smith for ferret tissue, Mohammad Rabiei for sectioning and staining $PV^{Cre};R26^{LSL\text{-}tdTom}$ tissue, and Varun Chokshi and Jeong Jun Kim for comments. The study was supported by NIH grants R01NS089652, 1R01NS104834–01, and 1RF1NS131984–01 (to D.H.O.) and by the intramural program of NIH, National Center for Complementary and Integrative Health, and National Institute of Neurological Disorders and Stroke (to A.T.C.).

REFERENCES

1. Pippi R, Spota A, and Santoro M (2018). Medicolegal Considerations Involving Iatrogenic Lingual Nerve Damage. J. Oral Maxillofac. Surg. 76, 1651.e1–1651.e13. 10.1016/j.joms.2018.03.020.
2. Tei K, Yamazaki Y, Kobayashi M, Izumiyama Y, Ono M, and Totsuka Y (2004). Effects of bilateral lingual and inferior alveolar nerve anesthesia effects on masticatory function and early swallowing. Oral Surg. Oral Med. Oral Pathol. Oral Radiol. Endod. 97, 553–558. 10.1016/S1079210403006875. [PubMed: 15153865]
3. Chee C, Arshad S, Singh S, Mistry S, and Hamdy S (2005). The influence of chemical gustatory stimuli and oral anaesthesia on healthy human pharyngeal swallowing. Chem. Senses 30, 393–400. 10.1093/chemse/bji034. [PubMed: 15829608]
4. Stern JM, and Johnson SK (1989). Perioral somatosensory determinants of nursing behavior in Norway rats (Rattus norvegicus). J. Comp. Psychol. 103, 269–280. 10.1037/0735-7036.103.3.269. [PubMed: 2776423]
5. Niemi M, Laaksonen J-P, Vähätalo K, Tuomainen J, Aaltonen O, and Happonen R-P (2002). Effects of transitory lingual nerve impairment on speech: an acoustic study of vowel sounds. J. Oral Maxillofac. Surg. Off. J. Am. Assoc. Oral Maxillofac. Surg. 60, 647–652. 10.1053/joms.2002.33113.
6. Blom S (1960). Afferent influences on tongue muscle activity. A morphological and physiological study in the cat. Acta Physiol. Scand. Suppl.49, 1–97.
7. Trulsson M, and Essick GK (1997). Low-threshold mechanoreceptive afferents in the human lingual nerve. J. Neurophysiol. 77, 737–748. 10.1152/jn.1997.77.2.737. [PubMed: 9065846]
8. Trulsson M, and Essick GK (2010). Sensations Evoked by Microstimulation of Single Mechanoreceptive Afferents Innervating the Human Face and Mouth. J. Neurophysiol. 103, 1741–1747. 10.1152/jn.01146.2009. [PubMed: 20130037]
9. Aktar T, Chen J, Ettelaie R, and Holmes M (2015). Tactile Sensitivity and Capability of Soft-Solid Texture Discrimination. J. Texture Stud. 46, 429–439. 10.1111/jtxs.12142.
10. Miles BL, Van Simaeys K, Whitecotton M, and Simons CT (2018). Comparative tactile sensitivity of the fingertip and apical tongue using complex and pure tactile tasks. Physiol. Behav. 194, 515–521. 10.1016/j.physbeh.2018.07.002. [PubMed: 29981764]
11. Abraira VE, and Ginty DD (2013). The sensory neurons of touch. Neuron 79, 618–639. 10.1016/j.neuron.2013.07.051. [PubMed: 23972592]
12. Reginato G.d.S., Bolina C.d.S., Watanabe I.s., and Ciena AP (2014). Three-Dimensional Aspects of the Lingual Papillae and Their Connective Tissue Cores in the Tongue of Rats: A Scanning Electron Microscope Study. Sci. World J. 2014, 841879. 10.1155/2014/841879.
13. Gozdziewska-Har1ajczuk K, Kleckowska-Nawrot J, Barszcz K, Marycz K, Nawara T, Modlinska K, and Stryjek R (2018). Biological aspects of the tongue morphology of wild-captive WWCPS rats: a histological, histochemical and ultrastructural study. Anat. Sci. Int. 93, 514–532. 10.1007/s12565-018-0445-y. [PubMed: 29948977]
14. Wang Y, Williams J, Rattner A, Wu S, Bassuk AG, Goffinet AM, and Nathans J (2016). Patterning of papillae on the mouse tongue: A system for the quantitative assessment of planar cell polarity signaling. Dev. Biol. 419, 298–310. 10.1016/j.ydbio.2016.09.004. [PubMed: 27612405]
15. Böck P (1971). Nerves of the papilla filiformis of the tongue of the guinea pig. Arch. Histol. Jpn. Nihon Soshikigaku Kiroku 32, 399–411.
16. Kunze K (1969). The filiform papilla in man as a tactile sense organ. Light and electron microscopic studies. Ergeb. Anat. Entwicklungsgesch. 41, 3–64.

17. Sato O, Maeda T, Kobayashi S, Iwanaga T, and Fujita T (1988). Filiform papillae as a sensory apparatus in the tongue: An immunohistochemical study of nervous elements by use of neurofilament protein (NFP) and S-100 protein antibodies. Cell Tissue Res. 252, 231–238. 10.1007/BF00214365. [PubMed: 3133113]

18. Lauga E, Pipe CJ, and Le Révérend B (2016). Sensing in the Mouth: A Model for Filiform Papillae as Strain Amplifiers. Front. Physiol. 4, 35. 10.3389/fphy.2016.00035.

19. Ranade SS, Woo S-H, Dubin AE, Moshourab RA, Wetzel C, Petrus M, Mathur J, Bégay V, Coste B, Mainquist J, et al. (2014). Piezo2 is the major transducer of mechanical forces for touch sensation in mice. Nature 516, 121–125. 10.1038/nature13980. [PubMed: 25471886]

20. Chesler AT, Szczot M, Bharucha-Goebel D, Čeko M, Donkervoort S, Laubacher C, Hayes LH, Alter K, Zampieri C, Stanley C, et al. (2016). The Role of PIEZO2 in Human Mechanosensation. N. Engl. J. Med. 375, 1355–1364. 10.1056/NEJMoa1602812. [PubMed: 27653382]

21. Moayedi Y, Duenas-Bianchi LF, and Lumpkin EA (2018). Somatosensory innervation of the oral mucosa of adult and aging mice. Sci. Rep. 8, 9975. 10.1038/s41598-018-28195-2. [PubMed: 29967482]

22. Yackinous C, and Guinard J-X (2001). Relation between PROP taster status and fat perception, touch, and olfaction. Physiol. Behav. 72, 427–437. 10.1016/S0031-9384(00)00430-3. [PubMed: 11274688]

23. Essick GK, Chopra A, Guest S, and McGlone F (2003). Lingual tactile acuity, taste perception, and the density and diameter of fungiform papillae in female subjects. Physiol. Behav. 80, 289–302. 10.1016/j.physbeh.2003.08.007. [PubMed: 14637228]

24. Bangcuyo RG, and Simons CT (2017). Lingual tactile sensitivity: effect of age group, sex, and fungiform papillae density. Exp. Brain Res. 235, 2679–2688. 10.1007/s00221-017-5003-7. [PubMed: 28589232]

25. Zhou X, Yeomans M, Thomas A, Wilde P, Linter B, and Methven L (2021). Individual differences in oral tactile sensitivity and gustatory fatty acid sensitivity and their relationship with fungiform papillae density, mouth behaviour and texture perception of a food model varying in fat. Food Qual. Prefer. 90, 104116. 10.1016/j.foodqual.2020.104116.

26. Donnelly CR, Kumari A, Li L, Vesela I, Bradley RM, Mistretta CM, and Pierchala BA (2022). Probing the multimodal fungiform papilla: complex peripheral nerve endings of chorda tympani taste and mechanosensitive fibers before and after Hedgehog pathway inhibition. Cell Tissue Res. 387, 225–247. 10.1007/s00441-021-03561-1. [PubMed: 34859291]

27. Donnelly CR, Shah AA, Mistretta CM, Bradley RM, and Pierchala BA (2018). Biphasic functions for the GDNF-Ret signaling pathway in chemosensory neuron development and diversification. Proc. Natl. Acad. Sci. USA 115, E516–E525. 10.1073/pnas.1708838115. [PubMed: 29282324]

28. Yokota Y, and Bradley RM (2016). Receptive field size, chemical and thermal responses, and fiber conduction velocity of rat chorda tympani geniculate ganglion neurons. J. Neurophysiol. 115, 3062–3072. 10.1152/jn.00045.2016. [PubMed: 27030734]

29. Fei D, Huang T, and Krimm RF (2014). The neurotrophin receptor p75 regulates gustatory axon branching and promotes innervation of the tongue during development. Neural Dev. 9, 15. 10.1186/1749-8104-9-15. [PubMed: 24961238]

30. Suemune S, Nishimori T, Hosoi M, Suzuki Y, Tsuru H, Kawata T, Yamauchi K, and Maeda N (1992). Trigeminal nerve endings of lingual mucosa and musculature of the rat. Brain Res. 586, 162–165. 10.1016/0006-8993(92)91389-V. [PubMed: 1380878]

31. Ohman-Gault L, Huang T, and Krimm R (2017). The transcription factorPhox2b distinguishes between oral and non-oral sensory neurons in the geniculate ganglion. J. Comp. Neurol. 525, 3935–3950. 10.1002/cne.24312. [PubMed: 28856690]

32. Spassova I (1974). Ultrastructure of the simple encapsulated nerve endings (simple end-bulbs of Krause) in the tongue of the cat. J. Anat. 118, 1–9. [PubMed: 4426873]

33. Takemura A, Uemura M, Toda I, Fang G, Hikida M, and Suwa F (2009). Morphological study of the lingual papillae in the ferret (Mustela putorius furo). Okajimas Folia Anat. Jpn. 86, 17–24. 10.2535/ofaj.86.17. [PubMed: 19522302]

34. Godement P, Vanselow J, Thanos S, and Bonhoeffer F (1987). A study in developing visual systems with a new method of staining neurones and their processes in fixed tissue. Dev. Camb. Engl. 101, 697–713. 10.1242/dev.101.4.697.
35. Honig MG, and Hume RI (1986). Fluorescent carbocyanine dyes allow living neurons of identified origin to be studied in long-term cultures. J. Cell Biol. 103, 171–187. 10.1083/jcb.103.1.171. [PubMed: 2424918]
36. Wu A, Dvoryanchikov G, Pereira E, Chaudhari N, and Roper SD (2015). Breadth of tuning in taste afferent neurons varies with stimulus strength. Nat. Commun. 6, 8171. 10.1038/ncomms9171. [PubMed: 26373451]
37. Leijon SCM, Neves AF, Breza JM, Simon SA, Chaudhari N, and Roper SD (2019). Oral thermosensing by murine trigeminal neurons: modulation by capsaicin, menthol and mustard oil. J. Physiol. 597, 2045–2061. 10.1113/JP277385. [PubMed: 30656684]
38. Kim AY, Tang Z, Liu Q, Patel KN, Maag D, Geng Y, and Dong X (2008). Pirt, a phosphoinositide-binding protein, functions as a regulatory subunit of TRPV1. Cell 133, 475–485. 10.1016/j.cell.2008.02.053. [PubMed: 18455988]
39. Patel KN, Liu Q, Meeker S, Undem BJ, and Dong X (2011). Pirt, aTRPV1 modulator, is required for histamine-dependent and -independent itch. PLoS One 6, e20559. 10.1371/journal.pone.0020559. [PubMed: 21655234]
40. Kim YS, Anderson M, Park K, Zheng Q, Agarwal A, Gong C, Young L, He S, LaVinka PC, Zhou F, et al. (2016). Coupled Activation of Primary Sensory Neurons Contributes to Chronic Pain. Neuron 91, 1085–1096. 10.1016/j.neuron.2016.07.044. [PubMed: 27568517]
41. Vandenbeuch A, Tizzano M, Anderson CB, Stone LM, Goldberg D, and Kinnamon SC (2010). Evidence for a role of glutamate as an efferent transmitter in taste buds. BMC Neurosci. 11, 77. 10.1186/1471-2202-11-77. [PubMed: 20565975]
42. Kim YS, Kim TH, McKemy DD, and Bae YC (2015). Expression of vesicular glutamate transporters in transient receptor potential melastatin 8 (TRPM8)-positive dental afferents in the mouse. Neuroscience 303, 378–388. 10.1016/j.neuroscience.2015.07.013. [PubMed: 26166724]
43. Lagerström MC, Rogoz K, Abrahamsen B, Persson E, Reinius B, Nordenankar K, Olund C, Smith C, Mendez JA, Chen Z-F, et al. (2010). VGLUT2-dependent sensory neurons in the TRPV1 population regulate pain and itch. Neuron 68, 529–542. 10.1016/j.neuron.2010.09.016. [PubMed: 21040852]
44. Schöbel N, Radtke D, Kyereme J, Wollmann N, Cichy A, Obst K, Kallweit K, Kletke O, Minovi A, Dazert S, et al. (2014). Astringency is a trigeminal sensation that involves the activation of G protein-coupled signaling by phenolic compounds. Chem. Senses 39, 471–487. 10.1093/chemse/bju014. [PubMed: 24718416]
45. Luo J, Ke J, Hou X, Li S, Luo Q, Wu H, Shen G, and Zhang Z (2022). Composition, structure and flavor mechanism of numbing substances in Chinese prickly ash in the genus Zanthoxylum: A review. Food Chem. 373, 131454. 10.1016/j.foodchem.2021.131454. [PubMed: 34731789]
46. Kuroki S, Hagura N, Nishida S, Haggard P, and Watanabe J (2016). Sanshool on The Fingertip Interferes with Vibration Detection in a Rapidly-Adapting (RA) Tactile Channel. PLoS One 11, e0165842. 10.1371/journal.pone.0165842. [PubMed: 27935970]
47. Moayedi Y, Michlig S, Park M, Koch A, and Lumpkin EA (2021). Somatosensory innervation of healthy human oral tissues. J. Comp. Neurol. 529, 3046–3061. 10.1002/cne.25148. [PubMed: 33786834]
48. Handler A, and Ginty DD (2021). The mechanosensory neurons of touch and their mechanisms of activation. Nat. Rev. Neurosci. 22, 521–537. 10.1038/s41583-021-00489-x. [PubMed: 34312536]
49. Kuehn ED, Meltzer S, Abraira VE, Ho C-Y, and Ginty DD (2019). Tiling and somatotopic alignment of mammalian low-threshold mechanoreceptors. Proc. Natl. Acad. Sci. USA 116, 9168–9177. 10.1073/pnas.1901378116. [PubMed: 30996124]
50. Li L, Rutlin M, Abraira VE, Cassidy C, Kus L, Gong S, Jankowski MP, Luo W, Heintz N, Koerber HR, et al. (2011). The functional organization of cutaneous low-threshold mechanosensory neurons. Cell 147, 1615–1627. 10.1016/j.cell.2011.11.027. [PubMed: 22196735]

51. Ikeda R, Cha M, Ling J, Jia Z, Coyle D, and Gu JG (2014). Merkel cells transduce and encode tactile stimuli to drive Aβ-afferent impulses. Cell 157, 664–675. 10.1016/j.cell.2014.02.026. [PubMed: 24746027]
52. Maksimovic S, Nakatani M, Baba Y, Nelson AM, Marshall KL, Wellnitz SA, Firozi P, Woo S-H, Ranade S, Patapoutian A, and Lumpkin EA (2014). Epidermal Merkel cells are mechanosensory cells that tune mammalian touch receptors. Nature 509, 617–621. 10.1038/nature13250. [PubMed: 24717432]
53. Tang T, and Pierchala BA (2022). Oral Sensory Neurons of the Geniculate Ganglion That Express Tyrosine Hydroxylase Comprise a Subpopulation That Contacts Type II and Type III Taste Bud Cells. eNeuro 9. 10.1523/ENEURO.0523-21.2022.
54. Nagy JI, Goedert M, Hunt SP, and Bond A (1982). The nature of the substance P-containing nerve fibres in taste papillae of the rat tongue. Neuroscience 7, 3137–3151. 10.1016/0306-4522(82)90236-6. [PubMed: 6186943]
55. Whitehead MC, Beeman CS, and Kinsella BA (1985). Distribution of taste and general sensory nerve endings in fungiform papillae of the hamster. Am. J. Anat. 173, 185–201. 10.1002/aja.1001730304. [PubMed: 20726120]
56. Moayedi Y, Xu S, Obayashi SK, Hoffman BU, Gerling GJ, and Lumpkin EA (2023). The cellular basis of mechanosensation in mammalian tongue. Cell Rep. 42, 112087. 10.1016/j.celrep.2023.112087. [PubMed: 36763499]
57. Wang Y, Erickson RP, and Simon SA (1993). Selectivity of lingual nerve fibers to chemical stimuli. J. Gen. Physiol. 101, 843–866. 10.1085/jgp.101.6.843. [PubMed: 8331321]
58. Bautista DM, Siemens J, Glazer JM, Tsuruda PR, Basbaum AI, Stucky CL, Jordt S-E, and Julius D (2007). The menthol receptor TRPM8 is the principal detector of environmental cold. Nature 448, 204–208. 10.1038/nature05910. [PubMed: 17538622]
59. von Buchholtz LJ, Ghitani N, Lam RM, Licholai JA, Chesler AT, and Ryba NJP (2021). Decoding Cellular Mechanisms for Mechanosensory Discrimination. Neuron 109, 285–298.e5. 10.1016/j.neuron.2020.10.028. [PubMed: 33186546]
60. Nguyen MQ, Wu Y, Bonilla LS, von Buchholtz LJ, and Ryba NJP (2017). Diversity amongst trigeminal neurons revealed by high throughput single cell sequencing. PLoS One 12, e0185543. 10.1371/journal.pone.0185543. [PubMed: 28957441]
61. Bai L, Lehnert BP, Liu J, Neubarth NL, Dickendesher TL, Nwe PH, Cassidy C, Woodbury CJ, and Ginty DD (2015). Genetic identification of an expansive mechanoreceptor sensitive to skin stroking. Cell 163, 1783–1795. 10.1016/j.cell.2015.11.060. [PubMed: 26687362]
62. Wang C-M, Green DP, and Dong X (2022). Transcription Factor MAFA Regulates Mechanical Sensation by Modulating Piezo2 Expression. Neurosci. Bull. 38, 933–937. 10.1007/s12264-022-00879-w. [PubMed: 35585476]
63. Gautam M, Yamada A, Yamada AI, Wu Q, Kridsada K, Ling J, Yu H, Dong P, Ma M, Gu J, and Luo W (2024). Distinct local and global functions of mouse Aβ low-threshold mechanoreceptors in mechanical nociception. Nat. Commun. 15, 2911. 10.1038/s41467-024-47245-0. [PubMed: 38575590]
64. Arshadi C, Günther U, Eddison M, Harrington KIS, and Ferreira TA (2021). SNT: a unifying toolbox for quantification of neuronal anatomy. Nat. Methods 18, 374–377. 10.1038/s41592-021-01105-7. [PubMed: 33795878]
65. Tainaka K, Murakami TC, Susaki EA, Shimizu C, Saito R, Takahashi K, Hayashi-Takagi A, Sekiya H, Arima Y, Nojima S, et al. (2018). Chemical Landscape for Tissue Clearing Based on Hydrophilic Reagents. Cell Rep. 24, 2196–2210.e9. 10.1016/j.celrep.2018.07.056. [PubMed: 30134179]
66. Renier N, Wu Z, Simon DJ, Yang J, Ariel P, and Tessier-Lavigne M (2014). iDISCO: A Simple, Rapid Method to Immunolabel Large Tissue Samples for Volume Imaging. Cell 159, 896–910. 10.1016/j.cell.2014.10.010. [PubMed: 25417164]
67. Zocchi D, Wennemuth G, and Oka Y (2017). The cellular mechanism for water detection in the mammalian taste system. Nat. Neurosci. 20, 927–933. 10.1038/nn.4575. [PubMed: 28553944]

Highlights

- The tip of the tongue is heavily innervated by lingual mechanoreceptors
- Lingual LTMRs have small receptive fields and high sensitivity and adapt rapidly
- Lingual afferents exhibit distinct innervation patterns in different papilla types
- Fungiform papillae, the lingual papillae containing taste buds, are touch sensors

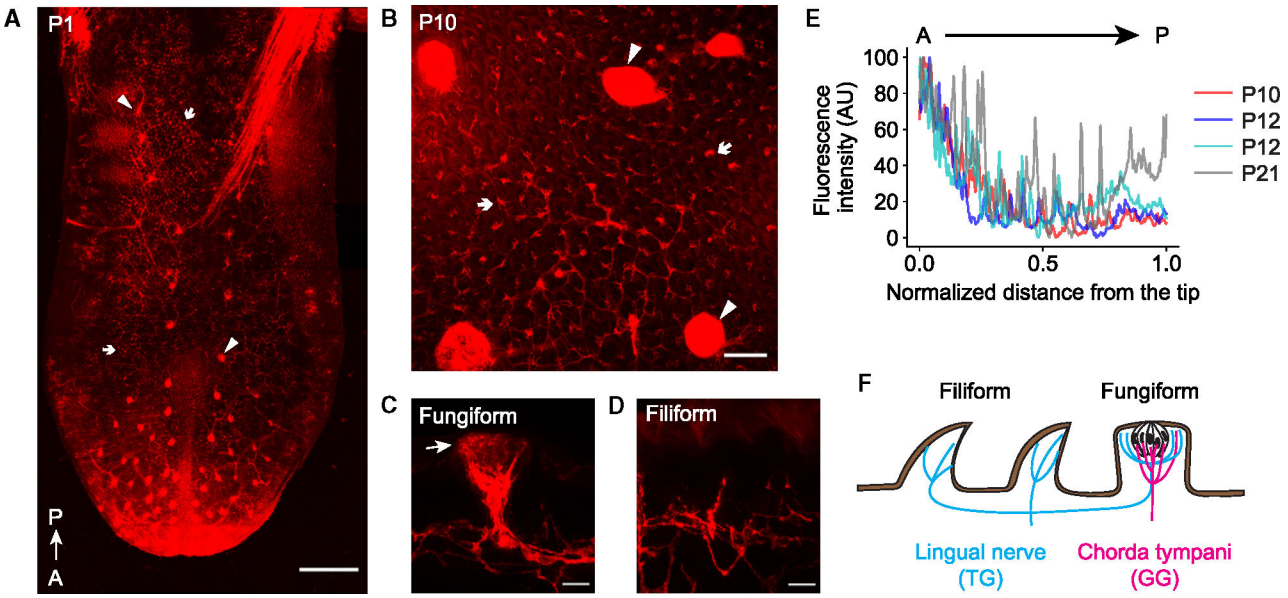

Figure 1. Trigeminal afferents innervate both filiform and fungiform papillae and have the highest density at the tongue tip

(A and B) Dorsal views of the tongue showing DiI-labeled trigeminal axons in P1 (A) and P10 (B) mice. Arrows: filiform; triangles: fungiform. To reveal the fluorescent signals in the filiform papillae in (B), those in the fungiform papillae are displayed saturated. Scale bars: 500 μm for (A) and 100 μm for (B).

(C and D) Longitudinal views of the tongue showing DiI-labeled trigeminal axons in fungiform (C) and filiform (D) papillae. Arrow in (C): axons terminating in extragemmal regions of a fungiform papilla. Scale bar: 20 μm. See also Figure S1.

(E) The fluorescence intensity along the A-P axis across DiI-labeled tongue surfaces at different ages.

(F) Schematic of the innervation patterns of TG neurons and GG neurons in filiform and fungiform papillae.

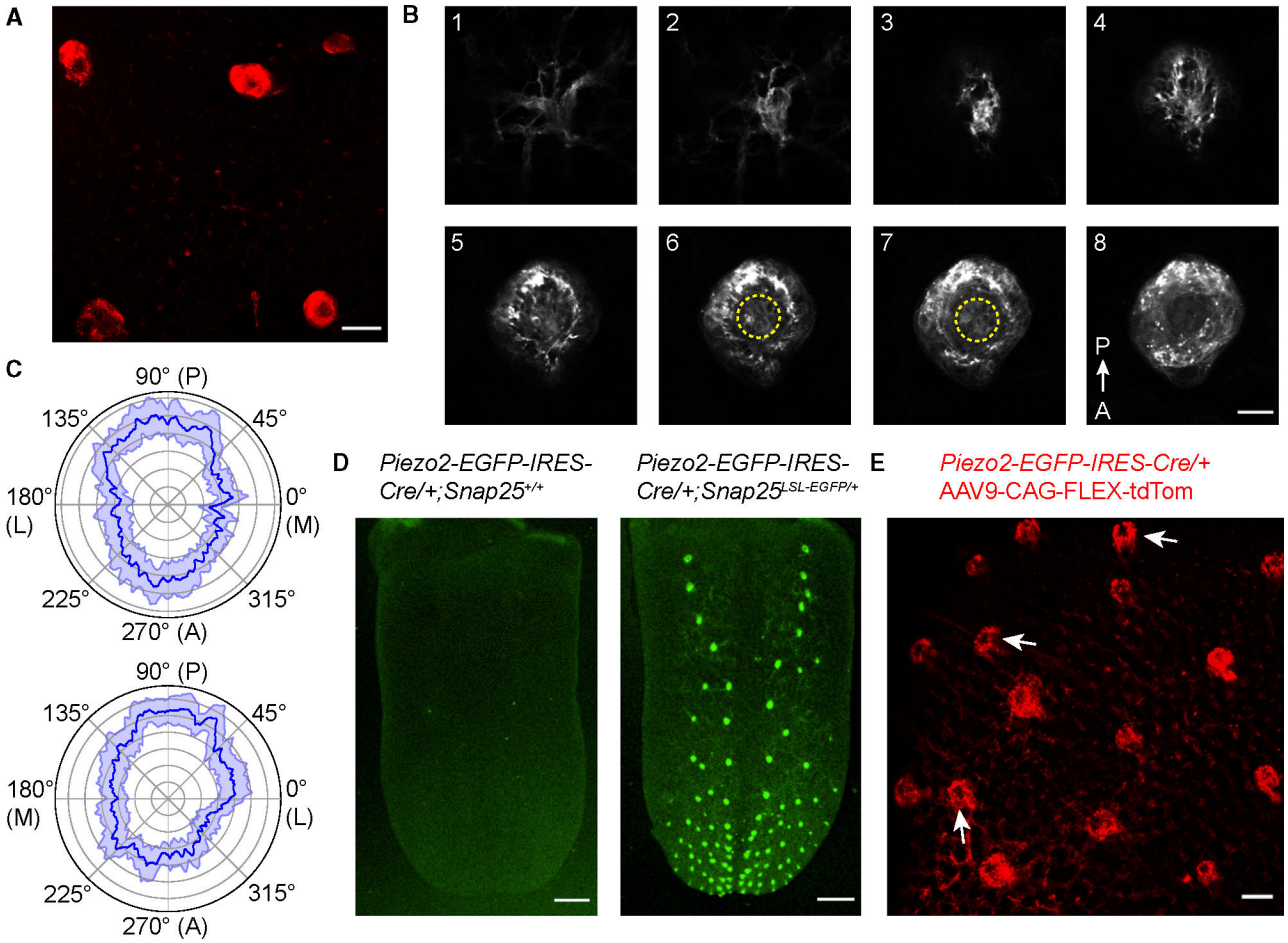

Figure 2. Trigeminal afferents asymmetrically innervate the extragemmal region of fungiform papillae and exhibit a ring-like termination pattern surrounding the taste pore, similar to Piezo2^{+} afferents

(A) Maximum intensity projection of the confocal z-stack in Figure 1B showing the ring-like innervation pattern of trigeminal afferents in fungiform papillae. Scale bar: 100 μm.

(B) Optical sections of DiI-labeled trigeminal afferents in a fungiform papilla from a top-down view. The sections are labeled in an order from the deeper connective tissue (section 1) to the apical epithelium (section 8). Yellow dashed lines: taste bud regions. Scale bar: 25 μm. See also Video S1.

(C) Fluorescence intensity of DiI in the ring region of fungiform papillae at each side of the tongue (top and bottom) on a linear scale (gray concentric circles). The dark blue line represents the mean intensity across fungiform papillae, while the light blue shading indicates the bootstrap 95% confidence interval. n = 26 and 27 papillae from 4 (2 P12 and 2 P21) mice for top and bottom, respectively.

(D) Dorsal view of the tongue in a *Piezo2-EGFP-IRES-Cre/+;Snap25*$^{LSL\text{-}EGFP/+}$ mouse and its *Piezo2-EGFP-IRES-Cre/+; Snap25*$^{+/+}$ littermate. Scale bar: 500 μm.

(E) Piezo2-expressing afferents innervate both fungiform and filiform papillae, and form a ring-like pattern (arrows) by innervating the extragemmal region of fungiform papillae. Scale bar: 100 μm.

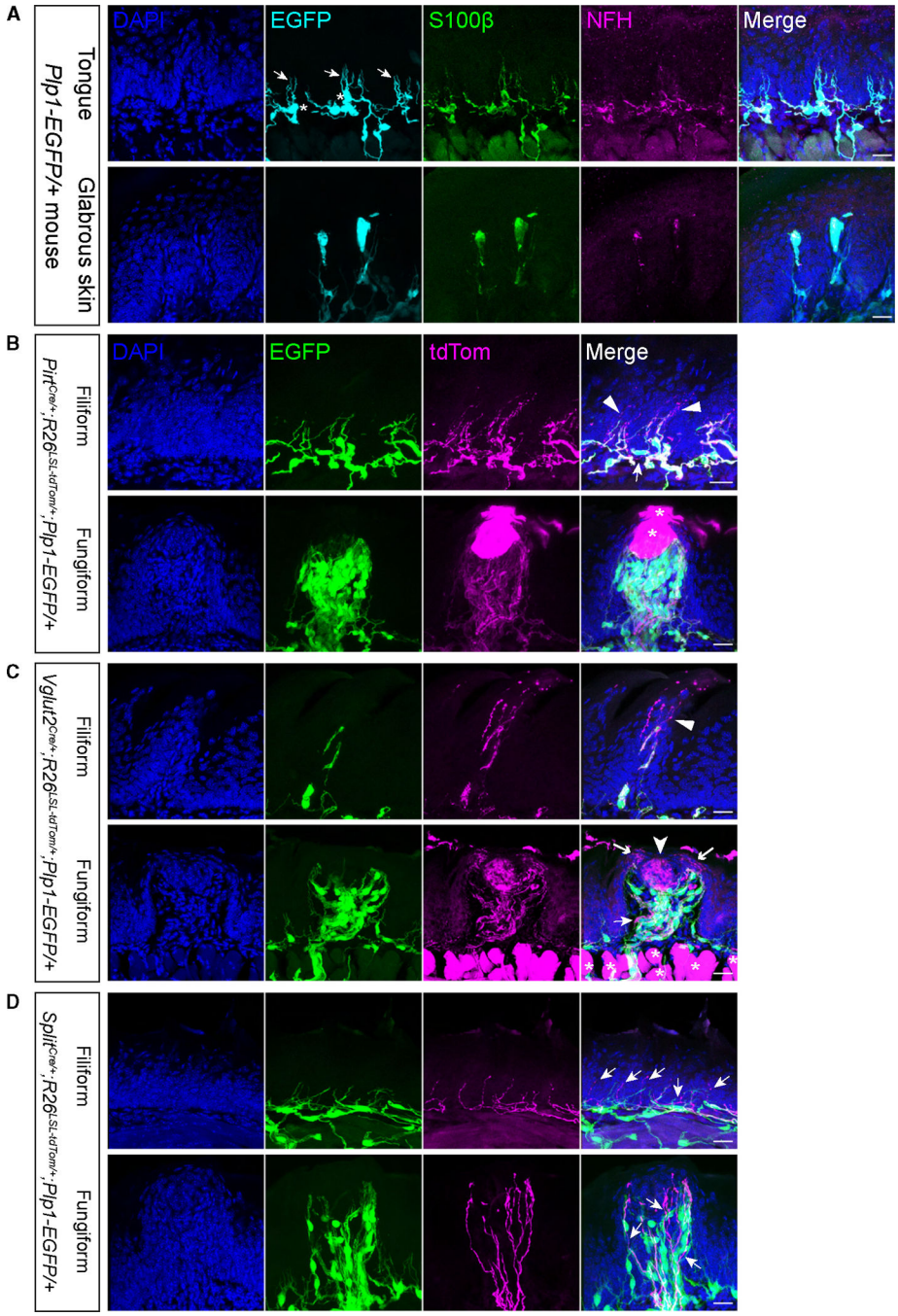

Figure 3. Mouse filiform papillae are innervated by NFH$^+$ myelinated free nerve endings

(A) Top: in the tongue of *Plp1-EGFP*/+ mice, no corpuscular end organs, but rather only myelinated free nerve endings, can be identified in the connective tissue core of filiform papillae. Bottom: in the glabrous skin, in contrast, Meissner corpuscles can be found in the dermal papillae. DAPI: cell nucleus. EGFP and S100β: (terminal) Schwann cells. Asterisks: cell bodies of Schwann cells. Arrows: cell processes or myelin from Schwann cells. See also Figure S2.

(B and C) In *Pirt*$^{Cre/+}$;*R26*$^{LSL\text{-}tdTom/+}$;*Plp1-EGFP*/+ and *Vglut2*$^{Cre/+}$;*R26*$^{LSL\text{-}tdTom/+}$;*Plp1-EGFP*/+ mice, tdTom-labeled, myelinated afferents that colocalized with EGFP can be seen in both filiform and fungiform papillae. (B) Asterisks: taste bud cells in and around fungiform papillae; triangles: the myelin was lost at the nerve terminal in myelinated afferents; thin arrows: unmyelinated afferents. (C) Asterisks: muscle; arrowhead: intragemmal afferents; thick arrows: extragemmal afferents; thin arrows: unmyelinated afferents.

(D) *Split*^{Cre} labeled unmyelinated afferents in both filiform and fungiform papillae (arrows). Scale bars in (A)–(D): 20 μm.

See also Figure S3 and Table S1.

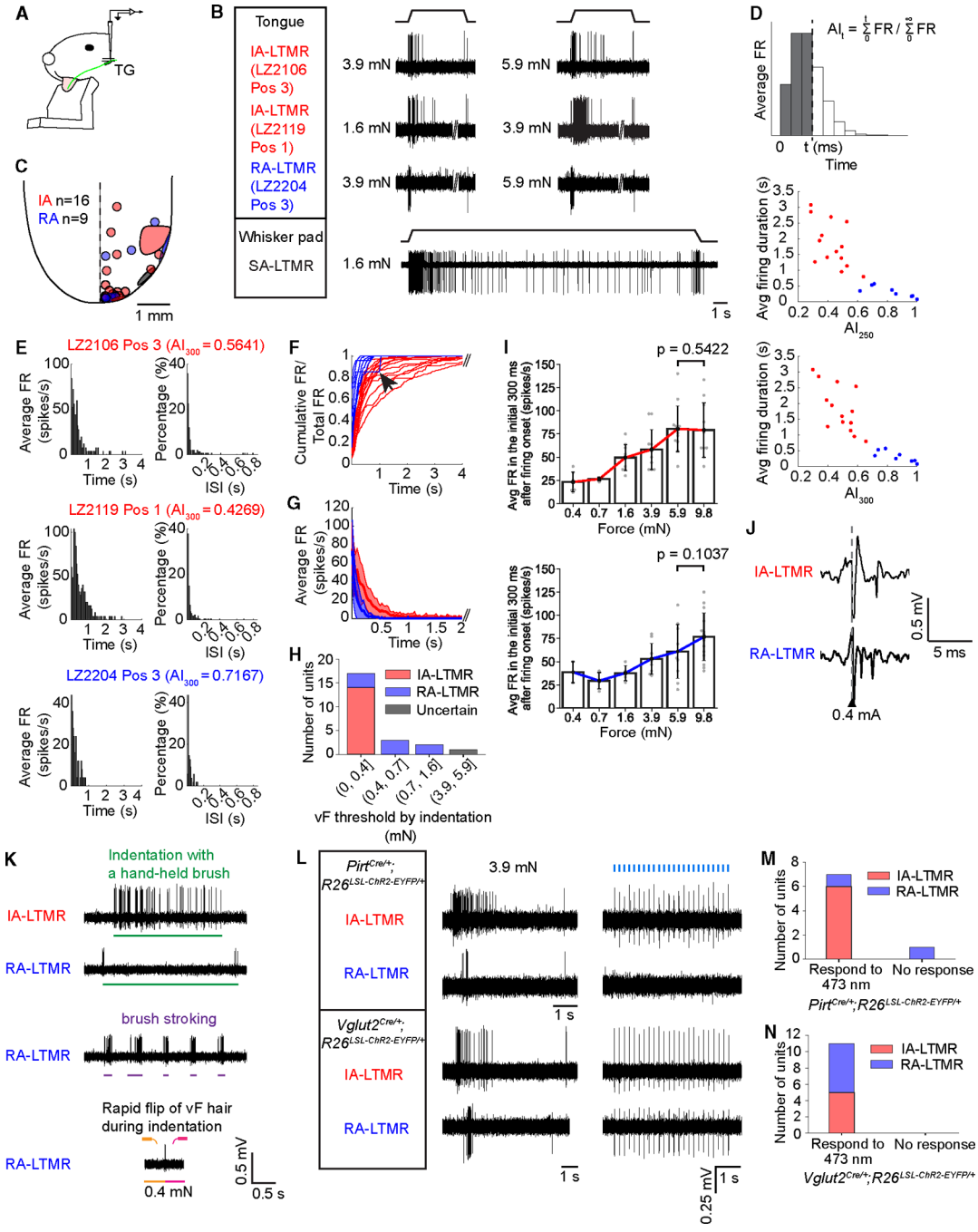

Figure 4. Single-unit recordings reveal lingual LTMRs ranging from RA to IA with varied tactile response properties

(A) The recording setup. Green: lingual nerve. See also Figure S4.

(B) Neural activity of single lingual LTMR units recorded in the TG in response to indentation at their RFs on the surface of the tongue. Neural traces with no spikes were cropped to make the onsets and offsets of indentation aligned for each column. An example SA-LTMR innervating the whisker pad was included for comparison.

(C) The RFs of lingual LTMRs mapped by von Frey hairs (n = 25 from 19 mice; 16 IA-LTMRs in red, 9 RA-LTMRs in blue, and 1 unit that cannot be categorized into IA/RA in gray).

(D) The AI and average firing duration of IA/RA-LTMRs for 3.9 mN stimulation. Top: schematic showing the calculation of AI_t using a peristimulus time histogram (PSTH) generated from a Poisson distribution.

(E) PSTHs (bin width: 50 ms, n = 5 events) and interspike intervals (ISIs, bin width: 10 ms) of the three example lingual units in (B) in response to 3.9 mN. See also Figure S5.

(F) Cumulative firing rate over total firing rate for IA/RA-LTMRs during 3.9 mN stimulation. Traces longer than 4 s were cropped. Arrow: an RA-LTMR with extremely low firing rates (LZ2203 Pos 6 Unit 3 in Figure S5B).

(G) Average firing rate of IA/RA-LTMRs during 3.9 mN stimulation (mean ± SD).

(H) The von Frey indentation threshold for lingual LTMRs (n = 23 from 16 mice; 14 IA-LTMRs, 8 RA-LTMRs, and 1 unit that could not be categorized).

(I) The average firing rates of an example IA-LTMR (left) and RA-LTMR (right) in the initial 300 ms after firing onset during indentation (mean ± SD; one-sided Student's t test).

(J) Example neural traces from conduction velocity tests. Gray dashed line: time point of the electrical pulse.

(K) Activity traces of lingual LTMRs in response to other tactile stimuli. The bottom row shows an RA-LTMR with a threshold higher than 0.4 mN.

(L) Neural activity of example single lingual LTMR units recorded in the TG in response to indentation and 473-nm light stimulation at their RFs. Blue bars: 10-msduration, 5 Hz, 473-nm light pulses.

(M and N) Number of lingual LTMR units that can or cannot be activated by 473-nm light stimulation from 3 $Pirt^{Cre/+};R26^{LSL\text{-}ChR2\text{-}EYFP/+}$ mice and 8 $Vglut2^{Cre/+};R26^{LSL\text{-}ChR2\text{-}EYFP/+}$ mice.

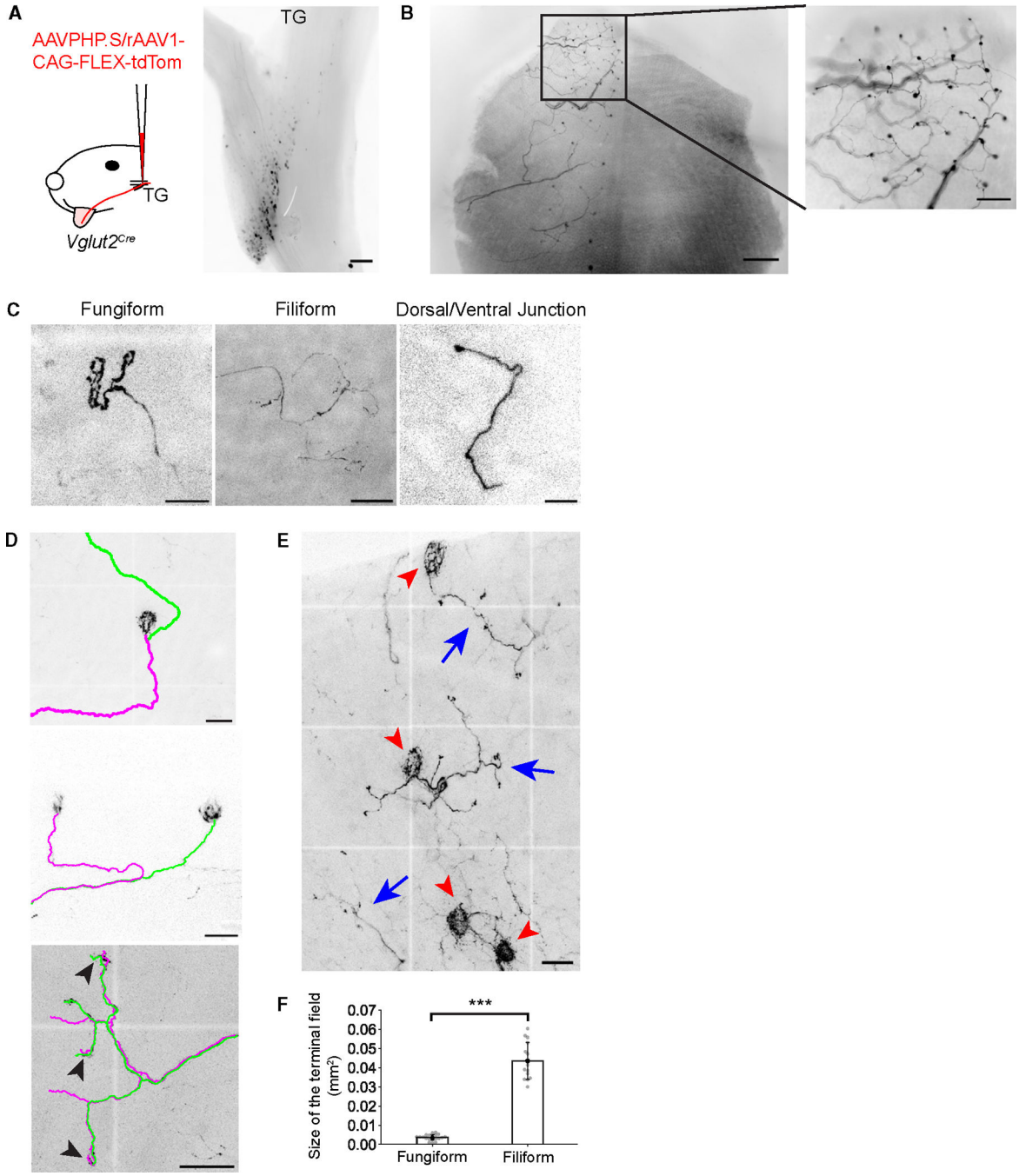

Figure 5. Lingual neurons that terminate in different types of papillae exhibit distinct terminal shapes and branching patterns

(A) Left: schematic of unilateral viral injection into the mandibular branch of the left TG in *Vglut2*^{Cre} mice. Right: neurons at the mandibular branch of the TG were labeled by tdTom. Scale bar: 300 μm.

(B) tdTom-labeled trigeminal afferents at the surface of the tongue. Scale bar: 800 μm. Inset: An enlarged view of the tip of the tongue. Scale bar: 300 μm.

(C) Single TG afferent terminals sparsely labeled by tdTom. Scale bars (left to right): 50, 100, and 50 μm.

(D) Multiple TG afferents simultaneously labeled by tdTom. Top: two clusters of nerve fibers (green and magenta) co-innervating a single fungiform papilla. Scale bar: 100 μm. Center: two independent afferents (green and magenta) innervating two separate fungiform papillae. Scale bar: 50 μm. Bottom: two independent afferents (green and magenta) innervating several filiform papillae had overlap in their terminal fields. Arrowheads: endings in the same filiform papillae. Scale bar: 100 μm.

(E) Clusters of filiform papillae innervated by separate TG afferent aggregates (blue arrows). Red arrowheads: fungiform papillae. Scale bar: 100 μm.

(F) The terminal field size of TG afferents innervating fungiform (0.0036 ± 0.0015, $n = 20$ from 5 mice) or filiform papillae (0.0435 ± 0.0096, $n = 14$ from 6 mice). ***$p = 9.59 \times 10^{-10}$; two-sided Welch's t test.

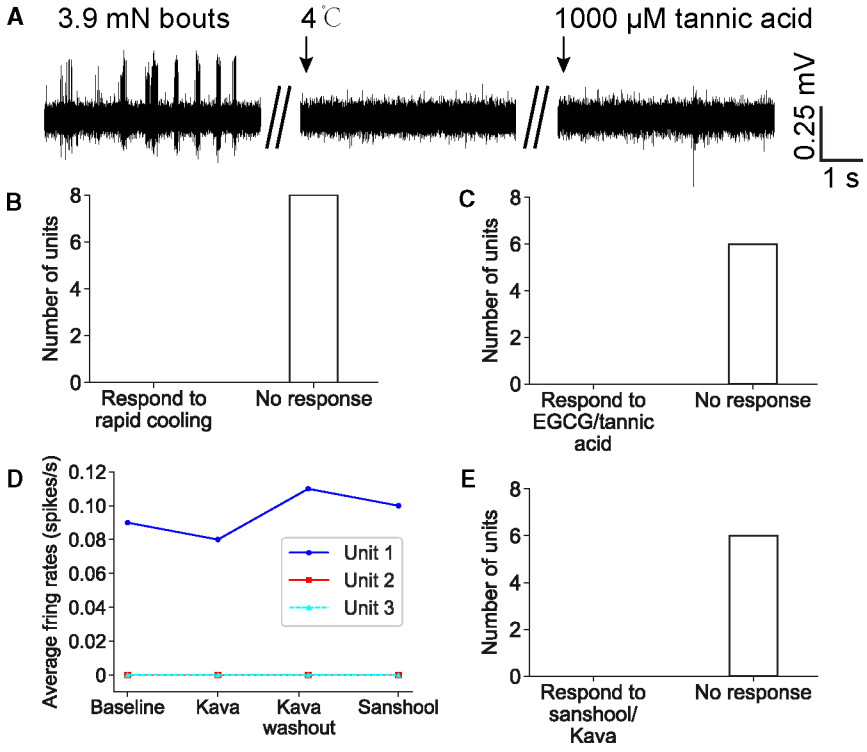

Figure 6. Lingual LTMRs are insensitive to rapid cooling or chemicals that can induce astringent or numbing sensations

(A) Activity of an example single lingual LTMR unitin the TG in response to indentation, rapid cooling, or tannic acid.

(B) Lingual LTMRs did not respond to rapid cooling ($n = 8$ from 6 mice).

(C) Lingual LTMRs did not respond to EGCG/tannicacid in a series of concentrations ($n = 6$ from 5 mice).

(D) The average firing rates of three example LTMRs before and during Kava/sanshool treatment (from 2 mice).

(E) Lingual LTMRs did not respond to sanshool or Kava ($n = 6$ from 4 mice).

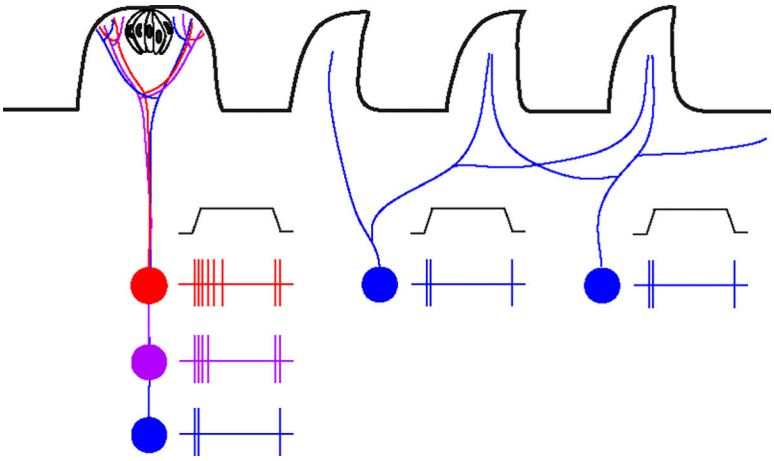

Figure 7. A working model of the organization of tactile innervation in the tongue

Schematic hypothesis of how the lingual papillae at the surface of the tongue could be innervated by lingual LTMRs in the TG. A single fungiform papilla is innervated by LTMRs ranging from IA to RA (red, purple, and blue), while several adjacent filiform papillae are simultaneously innervated by single RA-LTMRs (blue).

KEY RESOURCES TABLE

REAGENT or RESOURCE	SOURCE	IDENTIFIER
Antibodies		
Chicken anti-NFH	MilliporeSigma	Cat# AB5539; RRID: AB_11212161
Rabbit anti-S100	Abcam	Cat# AB76729; RRID: AB_1524357
Rabbit anti-S100	ProteinTech	Cat# 15146-1-AP; RRID: AB_2254244
Rabbit anti-PGP9.5	MilliporeSigma	Cat# AB1761-I; RRID: AB_2868444
Goat anti-Rabbit IgG Alexa Fluor 488	ThermoFisher	Cat# A-11008; RRID: AB_143165
Goat anti-Rabbit IgG Alexa Fluor 594	ThermoFisher	Cat# A-11012; RRID: AB_2534079
Goat anti-Rabbit IgG Alexa Fluor 647	ThermoFisher	Cat# A-21244; RRID: AB_2535812
Goat anti-Chicken IgY Alexa Fluor 488	ThermoFisher	Cat# A-11039; RRID: AB_2534096
Goat anti-Chicken IgY Alexa Fluor 647	ThermoFisher	Cat# A-21449; RRID: AB_2535866
Goat anti-Rat IgG Alexa Fluor 647	ThermoFisher	Cat# A-21247; RRID: AB_141778
Bacterial and virus strains		
AAV9-pCAG-FLEX-tdTomato-WPRE	Addgene	Cat# 51503
AAVPHP.S-CAG-FLEX-tdTomato	Addgene	Cat# 28306-PHP.S
rAAV1-CAG-FLEX-tdTomato	Addgene	Cat# 45282
Biological samples		
Mouse tissue (tongue, brain, trigeminal ganglion)	This paper	N/A
Ferret tissue (tongue)	This paper	N/A
Chemicals, peptides, and recombinant proteins		
DiIC18(3) (1,1'-dioctadecyl-3,3,3',3'-tetramethylindocarbocyanine perchlorate)	Invitrogen	Cat# D282
N-butyldiethanolamine	MilliporeSigma	Cat# 471240
Antipyrine	Tokyo Chemical Industry	Cat# D1876
Nicotinamide	Tokyo Chemical Industry	Cat# N0078
Hydroxy-α-sanshool	Medchemexpress	Cat# HY-N6825
Tannic acid	MilliporeSigma	Cat# 403040
(−)-epigallocatechin gallate (EGCG)	MilliporeSigma	Cat# E4143
Deposited data		
Data in MATLAB (.mat) and.csv format for this paper	This paper	Zenodo: https://doi.org/10.5281/zenodo.12802571
Experimental models: Organisms/strains		
Mice: *Plp1-EGFP* (B6; CBA-*Tg (Plp1-EGFP)10Wmac*/J)	The Jackson Laboratory	JAX: 033357; RRID: IMSR_JAX:033357
Mice: *Piezo2-EGFP-IRES-Cre* (B6(SJL)-*Piezo2*$^{tm1.1(cre)Apat}$/J)	The Jackson Laboratory	JAX: 027719; RRID: IMSR_JAX:027719
Mice: *Snap25-LSL-2A-EGFP-D* (B6.Cg-*Snap25*$^{tm1.1Hze}$/J)	The Jackson Laboratory	JAX: 021879; RRID: IMSR_JAX:021879

REAGENT or RESOURCE	SOURCE	IDENTIFIER
Mice: *Vglut2*$^{IRES\text{-}Cre}$ (B6J.129S6 (FVB)-*Slc17a6*$^{tm2(cre)Lowl}$/MwarJ)	The Jackson Laboratory	JAX: 028863; RRID: IMSR_JAX:028863
Mice: *Rosa26*^{Ai9} (B6.Cg-Gt(ROSA) *26Sor*$^{tm9(CAG\text{-}tdTomato)Hze}$/j)	The Jackson Laboratory	JAX: 007909; RRID: IMSR_JAX:007909
Mice: *Rosa26*^{Ai14} (B6.Cg-*Gt(ROSA) 26Sor*$^{tm14(CAG\text{-}tdTomato)Hze}$/j)	The Jackson Laboratory	JAX: 007914; RRID: IMSR_JAX:007914
Mice: *Rosa26*^{Ai32} (B6.Cg-*Gt(ROSA) 26Sor*$^{tm32(CAG\text{-}COP4*H134R/EYFP)Hze}$/J)	The Jackson Laboratory	JAX: 024109; RRID: IMSR_JAX:024109
Mice: *TrkB*^{CreERT2} (B6.129S6 (Cg)-*Ntrk2*$^{tm3.1(cre/ERT2)Dd9}$/J)	The Jackson Laboratory	JAX: 027214; RRID: IMSR_JAX:027214
Mice: *TrkC*^{CreERT2} (*Ntrk3*$^{tm3.\ 1(cre/ERT2)Dd9}$/J)[61]	The Jackson Laboratory	JAX: 030291; RRID: IMSR_JAX:030291
Mice: *Etv1*^{CreERT2} (B6(Cg)-*Etv* $^{tm1.1(cre/ERT2)Zjh}$/J)	The Jackson Laboratory	JAX: 013048; RRID: IMSR_JAX:013048
Mice: *Vglut1*$^{IRES2\text{-}Cre\text{-}D}$ (B6; 129S-*Slc17a7*$^{tm1.1(cre)Hze}$/J)	The Jackson Laboratory	JAX: 023527; RRID: IMSR_JAX:023527
Mice: *Advillin*^{Cre} (B6.129P2-*Avil*$^{tm2(cre)Eawa}$/J)	The Jackson Laboratory	JAX: 032536; RRID: IMSR_JAX:032536
Mice: *PV*^{Cre} (B6; 129P2-*Pvalb*$^{tm1(cre)Arbr}$/J)	The Jackson Laboratory	JAX: 017320; RRID: IMSR_JAX:017320
Mice: *TH*^{Cre} (B6.Cg-*7630403G23Rik*$^{T9(Th\text{–}cre)1Tmd}$/J)	The Jackson Laboratory	JAX: 008601; RRID: IMSR_JAX:008601
Mice: *MafA*^{Cre}	Wang et al., 2022[62]	N/A
Mice: *Pirt*^{Cre}	Kimetal., 2016[40]	N/A
Mice: *Split*^{Cre}	Gautam et al., 2024[63]	N/A
Mice: CD-1 (IGS)	Charles River Labs	CR: 022
Software and algorithms		
Fiji/ImageJ	NIH	https://imagej.net/software/fiji/
MATLAB versions R2019B and R2023a	MathWorks	RRID: SCR_001622
MClust 4.4	A. David Redish	https://github.com/adredish/MClust-Spike-Sorting-Toolbox
Polar Transformer (Fiji plugin)	Edwin Donnelly and Frederic Mothe	https://imagej.net/ij/plugins/polar-transformer.html
Python	Open Source	RRID: SCR_008394
SNT (Fiji plugin)	Arshadi et al., 2021[64]	https://imagej.net/plugins/snt/
WaveSurfer	HHMI Janelia Research Campus	https://wavesurfer.janelia.org/
Original analysis code	This paper	Zenodo:10.5281/zenodo.12802571
Other		
2 MΩ Tungsten microelectrode	World Precision Instruments	Cat# TM33A20
Amplifier: DAM80	World Precision Instruments	Cat# SYS-DAM80
Stimulus isolator	World Precision Instruments	Cat# A365
Concentric bipolar electrode	World Precision Instruments	Cat# TM33CCINS
473 nm DPSS laser	Laserglow Technologies	Cat# R471003GX